Healthy and diseased placental barrier on-a-chip models suitable for standardized studies

Rabussier, Gwenaëlle; Bünter, Ivan; Bouwhuis, Josse; Soragni, Camilla; van Zijp, Torben; Ng, Chee Ping

Published in:
Acta Biomaterialia

DOI:
10.1016/j.actbio.2023.04.033

Publication date:
2023

Acta Biomaterialia 164 (2023) 363–376

Contents lists available at ScienceDirect

Acta Biomaterialia

journal homepage: www.elsevier.com/locate/actbio

Full length article

Healthy and diseased placental barrier on-a-chip models suitable for standardized studies

Gwenaëlle Rabussier[a,b], Ivan Bünter[a], Josse Bouwhuis[a], Camilla Soragni[a,b], Torben van Zijp[a], Chee Ping Ng[a], Karel Domansky[a], Leon J. de Windt[b], Paul Vulto[a], Colin E. Murdoch[c], Kristin M. Bircsak[a], Henriëtte L. Lanz[a,*]

[a] MIMETAS BV, Oegstgeest, 2342 DH, the Netherlands
[b] Department of Cardiology, Maastricht University, Maastricht, 6226 ER, the Netherlands
[c] Systems Medicine, School of Medicine, University of Dundee, Dundee, DD1 9SY, Scotland, UK

ARTICLE INFO

Article history:
Received 5 October 2022
Revised 5 April 2023
Accepted 21 April 2023
Available online 26 April 2023

Keywords:
Disease modeling
Preeclampsia
Maternal-fetal interface
Standardized
Organ-on-a-chip

ABSTRACT

Pathologies associated with uteroplacental hypoxia, such as preeclampsia are among the leading causes of maternal and perinatal morbidity in the world. Its fundamental mechanisms are yet poorly understood due to a lack of good experimental models. Here we report an *in vitro* model of the placental barrier, based on co-culture of trophoblasts and endothelial cells against a collagen extracellular matrix in a microfluidic platform. The model yields a functional syncytium with barrier properties, polarization, secretion of relevant extracellular membrane components, thinning of the materno-fetal space, hormone secretion, and transporter function. The model is exposed to low oxygen conditions and perfusion flow is modulated to induce a pathological environment. This results in reduced barrier function, hormone secretion, and microvilli as well as an increased nuclei count, characteristics of preeclamptic placentas. The model is implemented in a titer plate-based microfluidic platform fully amenable to high-throughput screening. We thus believe this model could aid mechanistic understanding of preeclampsia and other placental pathologies associated with hypoxia/ischemia, as well as support future development of effective therapies through target and compound screening campaigns.

Statement of Significance

The human placenta is a unique organ sustaining fetal growth but is also the source of severe pathologies, such as preeclampsia. Though leading cause of perinatal mortality in the world, preeclampsia remains untreatable due to a lack of relevant *in vitro* placenta models. To better understand the pathology, we have developed 3D placental barrier models in a microfluidic device. The platform allows parallel culture of 40 perfused physiological miniaturized placental barriers, comprising a differentiated syncytium and endothelium that have been validated for transporter functions. Exposure to a hypoxic and ischemic environment enabled the mimicking of preeclamptic characteristics in high-throughput, which we believe could lead to a better understanding of the pathology as well as support future effective therapies development.

1. Introduction

In recent years, unpredictable and untreatable pregnancy disorders associated with uteroplacental hypoxia, such as gestational hypertension, intrauterine growth restriction and preeclampsia (PE) have emerged as major maternal and fetal health concerns [1,2]. Among those placental dysfunctions, preeclampsia is one of the leading causes of maternal and perinatal mortality and morbidity in the world [3]. It affects up to 8% of all pregnancies and contributes worldwide to 15% of maternal deaths annually [3,4]. Medical care costs associated with PE amount to an estimated $2.18 billion in the United States for the year of delivery and increase

* Corresponding author at: MIMETAS BV, Oegstgeest, 2342 DH, the Netherlands.
E-mail address: h.lanz@mimetas.com (H.L. Lanz).

https://doi.org/10.1016/j.actbio.2023.04.033

even further when long-term effects are considered [5]. PE is clinically defined by hypertension and proteinuria starting in the 20th week of pregnancy. Some of the severe complications include preterm delivery, organ damage, such as liver rupture or acute kidney failure, and cardiovascular disease [6]. Despite a rapid increase in PE incidence, as shown by a 25% increase between 1987 and 2004 in the United States [5], there are to date few reliable and early predicative biomarkers, preventive measures, or treatment strategies available. Today no cure is available, other than premature delivery of the fetus, which can be contributed to a poor understanding of the pathogenesis of PE [7].

It is well established that PE originates from the placenta [8]. As a unique and transient organ supporting pregnancy development, the placenta's main role is to provide essential nutrients and gasses, to mediate metabolic exchanges, as well as to protect the fetus from xenobiotics and pathogens [9]. The placenta bridges maternal and fetal circulation and is made up of a number of anatomical barriers, such as the syncytium, connective tissue and fetal capillaries [10]. The syncytium is in direct contact with maternal blood and constitutes the most important membrane barrier. It is comprised of a multinucleated layer of syncytiotrophoblasts originating from the fusion of underlying trophoblasts. The placenta is also a major source of hormone secretion, thereby playing a crucial role in maintaining a healthy pregnancy [11].

During pregnancy, the remodeling of the maternal spiral arteries by the end of the first trimester is essential for promoting adequate blood supply to the placenta and the fetus. It includes events such as trophoblast proliferation, differentiation and invasion [12]. Alterations in those events result in incomplete transformation of the spiral arteries leading to a reduction of the uteroplacental perfusion and subsequent placental ischemia and hypoxia [13,14]. Even though the trigger for abnormal placental development and the chronological order of events remains unknown, placental hypoperfusion is known to be accompanied by syncytium damage, impaired balance of angiogenic and anti-angiogenic factors, and release of pro-inflammatory molecules into the maternal circulation [15].

The poor understanding of PE and other uteroplacental associated diseases, lack of treatments and predictive biomarkers are mainly attributed to difficulties in studying the placenta, especially at the early stage of pregnancy. *Ex vivo* human placenta perfusion systems are the gold standard and have provided many clues regarding disease pathology [16]. However, they come with numerous limitations. The study of early stage of these pathologies is hampered by restrictions in access to placenta from terminated or unsuccessful pregnancies [17]. Animal models, such as mice and sheep have been useful in modeling localized physiological processes, but none of them exactly mirrors the human placenta pathology, resulting in poor translational relevance [18,19]. *In vitro* models have been developed utilizing immortalized cell lines, primary isolated trophoblast and placenta explants [20]. Their combination with manipulation of gene and protein expression as well as oxygen tension significantly helped elucidate key features of PE [21–23]. Nevertheless, trophoblast monolayer cell culture, conventional or in Transwell systems, lacks the multilayer complexity and dynamic environment of the placenta.

Culture of placenta cells in microfluidics system brought placental barrier modeling to a more advanced level. These organ-on-a-chip systems are enhancing tissue engineering by building more comprehensive tissues constituted of multiple cell types, extracellular matrix scaffolds, fluid flow and mechanical strain [24,25]. In recent years, several research groups have successfully developed placenta-on-a-chip models mimicking the multi-layered maternal-fetal interface. Models were utilized to reconstitute placenta physiology and study transplacental transfer of substances such as glucose [26,27], xenobiotics [28], caffeine [29] or nanoparticules [30,31]. Others have modeled placental inflammatory responses to bacterial infections [32].

Current placenta-on-a-chip models do have some limitations. The majority do not involve trophoblast cell line differentiation into syncytiotrophoblasts [27,29–34]. However, syncytium constitutes the main functional barrier of the placenta and is crucial to physiologically mimic the placental barrier. Also, none have reported to recreate the physiological maternal-fetal distance interface, primordial in the regulation of drug transfer between the mother and infant circulation. Moreover, chips are composed of polydimethylsiloxane (PDMS), known to absorb small hydrophobic molecules such as drugs [35]. Most importantly, these systems are typically low in throughput thus restricting the number of drugs that can be investigated. In addition, the use of microfluidics for the modeling of pregnancy disorders such as PE at the maternal-fetal interface level, has not been established yet.

Here, we report a robust and standardized approach for modeling the human placental barrier which addresses the drawbacks listed above and will greatly advance the field of *in vitro* placental modeling. The model comprises a multilayered functional syncytium and umbilical endothelium separated by a thin connective tissue-like extracellular matrix (ECM). We showed transporter functionality, barrier function and hormone secretion. To induce PE-like characteristics, we exposed our model to a hypoxic and ischemic environment. Under these conditions, the placental barrier on-a-chip showed a damaged syncytium, characterized by reduced barrier function and differentiation, down-regulation of glucose transporter-1 expression and reduction in angiogenic factors, which are all known to be features associated with uteroplacental hypoxia associated pathologies, such as PE [8,15,36,37]. Thus, our placental barrier on-a-chip model constitutes a promising tool for the studies of healthy and diseased pregnancy and opens the door for the evaluation of placental drug transfer and development of new therapeutics for the treatment of pregnancy disorders.

2. Materials and methods

2.1. Cell culture

Human choriocarcinoma cell line BeWo b30 clone (#C0030002; AddexBio) was cultured in T75 flasks in Optimized-DMEM (#C0003-02; AddexBio) supplemented with 10% fetal bovine serum (FBS; F4135; Sigma) and 1% penicillin-streptomycin (#15070063; Thermo Fisher). Cells were cultured in a humidified incubator (37 °C; 5% CO_2) and cell culture medium was changed every 2–3 days. After reaching 90% confluency, cells were trypsinized with 0.25% Trypsin-0.53 mM EDTA (#30–2101, ATCC) for passaging or seeding in the OrganoPlate.

Human umbilical vein endothelial cells from pooled donors (HUVEC; #C2519AS; Lonza) were thawed from liquid nitrogen and resuspended in Complete Human Endothelial Cell medium (#H116; Cell Biologics) for seeding in the OrganoPlate.

All experiments were performed with BeWo b30 and HUVEC cells between passages 26 to 30, and passage 4 to 5, respectively. The cells were routinely tested for mycoplasma contamination and found negative.

2.2. OrganoPlate culture

To recreate the multilayered architecture of the placental barrier, we used the Mimetas OrganoPlate 3-lane 40. This microfluidic device based on a standard 384-well microtiter plate (4004–400B; MIMETAS BV) contains 40 independent chips, enabling the parallel culture of as many organ models (Fig. 1A). Each tissue culture chip consists of three microfluidic lanes. The top and bottom perfusion lanes of 300 µm × 220 µm (w × h), and the middle lane of

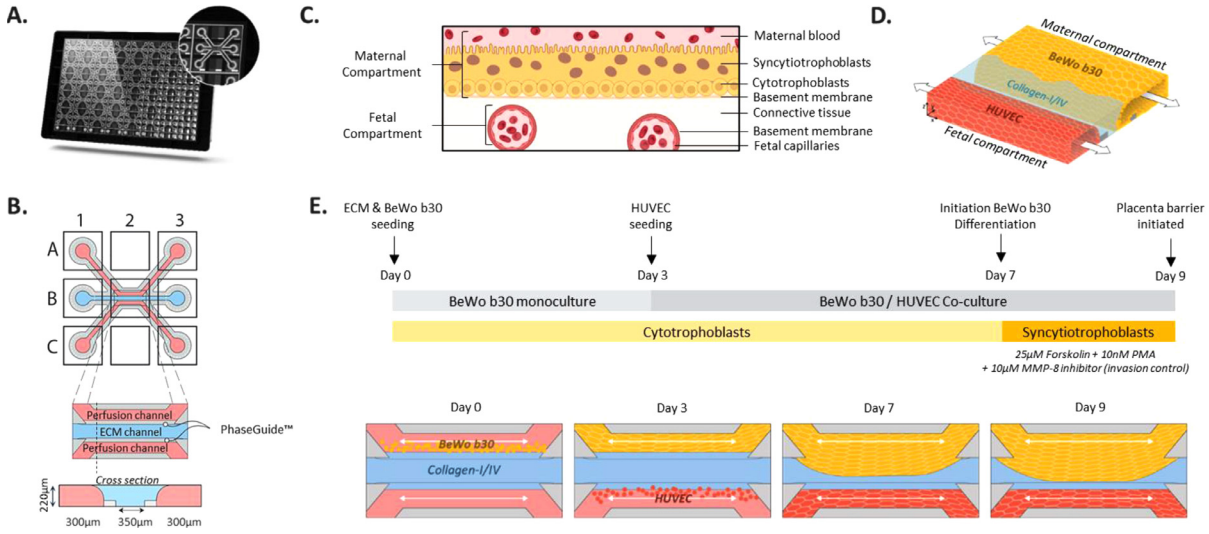

Fig. 1. Placental barrier on-a-chip set-up in the OrganoPlate 3-lane. (A) Bottom view of the OrganoPlate 3-lane, a 384-well plate format containing in its bottom 40 individual microfluidics chips. Zoomed-in image of one microfluidic chip. (B) Schematic representation of one chip consisting of three adjacent channels accessible by top (A1), bottom (C1) inlets and top (A3), bottom (C3) outlets wells. Perfusion channels are separated by small ridges (PhaseGuide™) which enabled the patterning of ECM gel in the middle lane and culture of cells in the perfusion channels in a membrane-free manner. Cultures are observed from the observation window (B2). (C) Schematic of the placental barrier multilayered architecture. The interface is composed of syncytiotrophoblasts and cytotrophoblasts (maternal compartment) on top of their basement membrane. A thin connective tissue separates the maternal interface from the fetal capillaries (fetal compartment). (D) 3-dimensional schematic of the placental barrier modeling in the OrganoPlate 3-lane, representing the maternal and fetal compartment in close proximity. Continuous flow through the maternal and fetal compartments is depicted by the arrows. (E) Schematic workflow depicting placental barrier modeling set-up, BeWo b30 differentiation and controlled invasion over time.

350 µm × 220 µm (w × h) are all accessible by their well openings. These channels are separated on their bottom by a meniscus pinning barrier, the PhaseGuide™ [38], allowing the patterning of extracellular matrix (ECM) gel in the middle channel and the culture of cells in the bordering perfusion channels in a membrane-free manner (Fig. 1B).

The first-trimester placenta is characterized by a trophoblast syncytium and its underlying cytotrophoblasts separated from the fetal endothelium by a thin connective tissue [9] (Fig. 1C). To model this maternal-fetal interface, the first-trimester trophoblast human choriocarcinoma cell line BeWo b30 and HUVEC are used to recreate the maternal and fetal compartment, respectively (Fig. 1D). Cells were cultured against a 3-dimensional ECM scaffold based of collagen-I and collagen-IV, key components of the placental barrier [39]. ECM was prepared by mixing independently and respectively, in 8:1:1 ratio, rat collagen-I 8.91 mg/mL (#354249; Corning) and collagen-IV from human placenta 5 mg/mL (#234154; Sigma-Aldrich) with HEPES (1 M; #15630; Life Technologies) and $NaHCO_3$ (37 g/L, S5761; Sigma-Aldrich) on ice. Collagen-I and collagen-IV ECM gels were then mixed in a 3:1 ratio. The collagen-I/collagen-IV ECM mixture was kept on ice and used for seeding within 10 min. Before ECM seeding, 50 µL HBSS (#H6648; Sigma-Aldrich) was added to the observation windows to prevent gel dehydration and to increase optical clarity. The ECM mixture (1.7 µL) was dispensed in the gel inlet. The plate was incubated in a humidified incubator (37 °C, 5% CO_2) for 15 min to allow the ECM to polymerize. For maternal compartment modeling, BeWo b30 cells were resuspended in their culture medium to a cell density of 12,000 cells/µL and 2 µL of cell suspension was added into the top perfusion inlet (Fig. 1E). Subsequently, 50 µL of BeWo b30 culture medium was added in the top and bottom inlet wells and the plate was placed on its side for 3 h to allow the cells to settle against the ECM. This was followed by addition of 50 µL medium to the top outlet, bottom inlet, and outlet wells. Bidirectional perfusion was started by placing the plate on a rocking platform (OrganoFlow; MIMETAS BV) set at a 7° inclination and 8-minute interval, in the incubator (37 °C, 5% CO_2). Medium was refreshed in top and bottom channels 2 days later. On day 3, fetal compartment modeling was initiated by HUVEC seeding into the bottom channel. Seeding of cells in channels previously wetted by medium was performed by passive pumping as previously described [40]. In short, medium was aspirated from top and bottom perfusion wells and bottom inlet to be seeded was washed with 50 µL PBS (#70013016; Thermo Fisher). 50 µL of endothelium was then dispensed on the bottom outlet and 2 µL of HUVEC suspension (10,000 cells/µL) was then seeded into the previously washed inlet. To avoid dehydration, 50 µL of BeWo culture medium was dispensed in the top channel outlet well and the plate was placed on its side for 1.5 h to allow the HUVEC to attach against the ECM. BeWo and HUVEC culture medium (50 µL) was respectively dispensed in top and bottom channel inlet wells. The OrganoPlate was placed back under perfusion in the incubator (37 °C, 5% CO_2). Cells were grown for several days under continuous perfusion. On day 6, medium was refreshed in top and bottom perfusion channel wells. After 7 days of culture, and to promote the differentiation of BeWo b30 into multinucleated syncytia, trophoblast cells were exposed for 48 h to 25 µM Forskolin (#F3917; Sigma-Aldrich), and 10 nM of Phorbol 12-myristate 13-acetate (PMA, #P1585; Sigma-Aldrich), well known activators of trophoblast differentiation pathways [41,42]. Additionally, BeWo b30 are known to secrete a wide range of metalloproteinases, characteristic of their invasiveness and ECM remodeling [43]. Because collagen-I is the main component of the ECM gel, BeWo b30 ECM invasion behavior was controlled and limited by supplementing trophoblast differentiation medium with 10 µM metalloproteinase-8 (MMP-8) inhibitor [44–46] (Figure S1). 50 µL of BeWo b30 differentiation medium (25 µM Forskolin, 10 nM PMA, 10 µM MMP-8 inhibitor) and HUVEC culture medium was refreshed on both days 7 and (Fig. 1E) 8 in the top perfusion channel and bottom perfusion wells, respectively. Placental barrier co-cultures were fully established after 9 days of culture, the main timepoint used for characterization and functionality assays in this study. Maternal and fetal compartments remained consistently distinct accross all cultures until 10 days (data not shown). From day 11–12 onwards, overgrowth of the trophoblats into the fetal com-

partment were observed in some chips. Placental barrier model is recommended to be used for assay performance between day 9 and day 10 of culture.

Preeclamptic characteristics were modelled by exposing placental barrier co-cultures to a hypoxic or hypoxic-ischemic environment. Co-cultures were established as described above and moved on day 8 to a low-oxygen incubator for 24 h (1% O_2, 37 °C, 5% CO_2). To model the "Hypoxic" condition, OrganoPlate were culture on the OrganoFlow (7°, 8-min intervals), while "Ischemic" condition was mimicked by placing plates flat and static.

Phase contrast images were taken every 1 to 3 days with a high content microscope (ImageXPress XLS-C; Molecular Devices) to monitor culture development.

2.3. Barrier integrity assay (BI assay)

From day 7 to day 9, the tightness of the trophoblast layer was assessed daily by monitoring the flux of fluorescent dyes from the apical to basal side of the tubule. The assay was previously described in intestinal epithelium tubes [47]. To ensure proper flow profiling, the gel inlet and outlet wells were washed with 25 µL endothelium culture medium for 5 min, under perfusion. Then, medium was aspirated from all wells of the chip and 20 µL of endothelium culture medium was dispensed in middle and bottom channel wells. Subsequently, 40 µL and 30 µL of medium containing 4.4 kDa TRITC-dextran (0.5 mg/mL; #T1037; Sigma-Aldrich) and sodium fluorescein (10 µg/mL; #F6377; Sigma) was dispensed in the top perfusion inlet and outlet wells, respectively. The passage of dextran into the basolateral side of the trophoblast layer was monitored every 2 min for 12 min with a high content microscope (ImageXPress XLS-C; Molecular Devices) in the TRITC and FITC channels. The ratio between the fluorescent signal in the basal and apical region of the tubule (leakage score) was calculated for each timepoint using Fiji Software [48].

2.4. TEER measurement

Transepithelial electrical resistance (TEER) of the trophoblast barrier was measured from day 6 to day 9 using an automated multichannel impedance spectrometer (OrganoTEER, MIMETAS) as previously published, providing electrical connections to all inlet and outlets well of the OrganoPlate [49]. Before measurement, 50 µL endothelium complete medium was refreshed in all perfusion channel wells and plate was kept static at room temperature (≈ 21 °C) for 30 min to ensure medium equilibration.

Using the OrganoTEER software (MIMETAS), impedance spectra of our tubes was measured (medium settings, 40 frequency points from 10 Hz to 150 kHz), from which the electrical resistance (Ohm) of the tubules were automatically extracted by the software fitting algorithm.

2.5. Immunofluorescent staining

Placental barrier cultures were fixed and prepared for immunostaining as previously described [47]. Briefly, 3.7% formaldehyde (#252549; Sigma) in HBSS (with $Ca^{+2}/Mg^{+\cdot}$) was added to the cultures for 15 min and rinsed with PBS. Cells were washed with a washing solution of 4% HI-FBS (#F4135; Sigma) in PBS and permeabilized with 0.3% Triton X-100 (#T8787; Sigma) for 10 min. Next, tubules were rinsed with washing solution and blocked with 2% HI-FBS, 2% BSA (#A2153; Sigma) and 0.1% Tween20 (#P9416; Sigma) in PBS for 45 min. The cells were then incubated with primary antibodies diluted in blocking solution overnight, static, at 4 °C. The following primary antibodies were used: Mouse anti-Ezrin (#610602; BD Transduction Laboratories; 1:100), Mouse anti-ZO-1 (#33–9100; Life Technologies; 1:125), Rabbit anti-ECAD (#3195S; Cell Signaling Technology; 1:200), Mouse anti-hCG-β (#ab958; Abcam; 1:100), Mouse anti-GLUT-1 (#ab40084; Abcam; 1:125), Rabbit anti-collagen-IV (#PA5-104508; Thermo Fisher; 1:100), Rabbit anti-laminin (#ab11575; Abcam; 1:200), Rat anti-perlecan (#MA106821; Thermo Fisher; 1:100), Rabbit anti-nidogen-2 (#PA5626615, Thermo Fisher, 1:500), Mouse anti-tenascin-C (#ab88280, Abcam, 1:500), Mouse anti-fibronectin Alexa Fluor 647 Conjugated (#56098; BD Biosciences; 1:200), Mouse isotype (#086599; Thermo Fisher), Rabbit isotype (#086199; Thermo Fisher) and Rat isotype (#96020201, Invitrogen). Cultures were washed three times with washing solution and then incubated for 30 min at room temperature on the OrganoFlow (7°, 2-min intervals) with Alexa Fluor 488 (#a32731; Invitrogen; 1:250) and Alexa Fluor 647 (#a31571; Life Technologies; 1:250) diluted in blocking buffer. Subsequently, cells were washed three times and nuclei were stained with Hoechst 33342 (#H3570; Thermo Fisher; 1:2000). Actin was stained using ActinGreen™ 488 ReadyProbes™ Reagent (#R37110; Thermo Fisher; 2 drops/mL) or ActinRed™ 555 ReadyProbes™ Reagent (#R37112; Thermo Fisher; 2 drops/mL) for 30 min at room temperature on the OrganoFlow (7°, 2-min intervals). For each immonstaining, the tested isotype controls did not show nonspecific binding. Chips were imaged on the High-Content Confocal Imaging System (ImageXPress® Micro Confocal; Molecular Devices). Immunostainings were processed using Fiji Software.

2.6. Maternal-fetal distance quantification

Placental barrier co-culture after 9 days of culture were fixed and permeabilized as previously described. Cultures were stained with ActinRed™ 555 ReadyProbes™ for 30 min on the OrganoFlow (7°, 2-min intervals). Z-stack from the bottom to the top of the chips were imaged on the High-Content Confocal Imaging System with 4x objective and maximum intensity projections were created.

ActinRed stained images were processed with built-in functions from the Fiji image processing package (version 2.0.0, build 1.52e) [48]. The contrast of the middle channels was enhanced by contrast limited adaptive histogram equalization (CLAHE, block size = 127, histogram bins = 256, maximum slope = 3) [50]. The middle channels were subsequently subjected to rolling ball background subtraction (radius = 50) to improve the signal-to-noise ratio and smoothed with a Gaussian blur (radius = 3) [51,52]. The processed images were binarized with the iterative self-organizing data analysis technique (ISODATA) [53]. The pixel intensity arrays were loaded into Python (version 3.9.10) to calculate the distances between the maternal and fetal epithelium cell layers of the defined region of interest (ROI) (Figure S2). Chips presenting maternal-fetal interface short distances below 20 µm, could not be quantified, and have been counted as 0 µm.

2.7. RNA extraction and quantitative real-time PCR (RT-qPCR)

Total RNA was extracted and isolated from BeWo b30 tubules using a RNeasy Mini Kit (#74004; QIAGEN). To specifically isolate RNA from trophoblast cells, endothelium was first lysed using RLT buffer, and cell lysate was aspirated. Next, BeWo b30 from 5 individual chips were lysed, pooled, and total RNA concentration was quantified with the NanoDrop OneC® spectrophotometer (Thermo Fisher). cDNA was synthetized using M-MLV reverse transcriptase (#28025013; Invitrogen). Quantitative real-time PCR (qPCR) was then performed using SYBR Green PCR Master Mix (#4309155; Thermo Fisher) with the LightCycler® 480 device (Roche). PCR primer sequences used for RT-qPCR are listed in Table 1. Target gene expression levels were normalized to GAPDH or Actin. Data were analyzed with the Roche, LightCycler software version 1.1.

Table 1
qPCR primer sequences.

Gene Name	Forward Primer Sequence (5′ to 3′)	Reverse Primer Sequence (5′ to 3′)
ERVFRD-1 (Syncytin-2)	CCAAATTCCCTCCTCTCCTC	CGGGTGTTAGTTTGCTTGGT
hCG-α	TTTCTGGTCACATTGTCGGT	TGGGCAATCCTGCACATCAG
hCG-β	CCTGGCCTTGTCTACCTCTT	GGCTTTATACCTCGGGGTTG
PlGF	CAGAGGTGGAAGTGGTACCCTTCC	CGGATCTTTAGGAGCTGCATGGTGAC
GAPDH	TTGACGCTGGGGCTGGCATT	GTGCTCTTGCTGGGGCTGGT
Actin	CTCTTCCAGCCTTCCTTCCT	AGCACTGTGTTGGCGTACAG

2.8. Human chorionic gonadotropin beta (hCG-β) quantification

BeWo culture medium from the top perfusion inlet and outlet wells was collected on day 7 (prior to trophoblast differentiation), day 8 (24 h post-differentiation) and day 9 (48 h post-differentiation) and stored at −80C° until assay was performed. The concentration of hCG-β in the culture medium was measured using the Human CG beta (HCG beta) Duoset ELISA (#DY9034-05, R&D Systems) according to the manufacturer protocol.

2.9. Drug transport activity assays

The transport activity of multidrug resistance-associated protein (MRP) transporters was assessed in the placental barrier on-a-chip as previously described [54]. Briefly, 30 µL of 1.25 µM 5-chloromethylfluorescein-diacetate (CMFDA, #C7025, Life Technologies) diluted in Opti-HBSS (1:2 Opti-MEM (#11058021, Gibco)) and HBSS) was added to all the perfusion inlets and outlets, either with two MRP inhibitors, MK571 (5 µM, 10 µM, 30 µM, #M7571, Sigma) and Quercetin [55,56] (30 µM, #Q4951, Sigma)) or their vehicle (DMSO, #D8418, Sigma). OrganoPlates were incubated in a humidified incubator (37 °C, 5% CO_2) for 30 min on the OrganoFlow (7°, 8-min intervals). Once inside the cell, CMFDA is metabolized to fluorescent compound MF-SG which is a substrate for MRPs. Cultures were then cooled down by adding 50 µL cold HBSS in the observation window. Assay solution was replaced with ice-cold inhibitor cocktail targeting MRP, BCRP and Pgp transporters (10 µM MK571, 10 µM Ko143 (#K2144, Sigma), 10 µM PSC833 (#SML0572, Sigma), respectively) [57,58] and was supplemented with 5 µg/mL Hoechst 33342 to measure total nuclei. Cultures were incubated 15 min under an angle, in the dark at RT and subsequently acquired.

A z-stack imaging of the bottom layers of the culture is performed using the High-Content Confocal Imaging System. SUM projections were processed using Fiji Software. MF-SG and Hoechst 33342 intracellular fluorescence were quantified and subtracted for background signal. The relative intensity was calculated by normalizing substrate intensity to the nuclei count.

2.10. Statistical analysis

All statistical analysis were performed using Prism 9 Software (GraphPad). Data are presented as mean ± standard deviation (SD) or mean ± standard error of mean (SEM) when specified. Two-tailed unpaired t-tests were performed to determine the significance between two independent groups. One-way analyses of variance (ANOVA), followed by Tukey's multiple comparisons test were performed when more than two groups were analyzed. Two-way ANOVA, followed by Tukey's multiple comparison, was performed when examining the influence of 2 independent variables. For multiple comparison tests, all groups were compared between each other's. Differences with $P < 0.05$ were considered as significant. * $P < 0.05$, ** $P < 0.01$, *** $P < 0.001$ and **** $P < 0.0001$.

3. Results

3.1. Establishment of a multicellular placental barrier on-a-chip with a physiologically relevant maternal-fetal interface

The maternal-fetal interface was established in the 3-lane OrganoPlate by co-culturing the human trophoblast cell line BeWo b30 and HUVEC (human umbilical vein endothelial cells) against a collagen-based scaffold (Fig. 1).

Phase contrast images showed that the BeWo b30 cells formed an epithelial barrier against the collagen-I/IV ECM gel after 3 days of culture, which progressed over time towards the vessel lane (Fig. 2A). BeWo b30 in co-culture with HUVEC (Fig. 2Aii) supported the maintenance of distinct maternal and fetal compartments. This compartmentalization was visualized by staining the epithelial maternal compartment for adherent junctions (ECAD), and both the epithelium and endothelium for Actin (Fig. 2B). A 3D reconstruction of the placental barrier model stained for Actin and tight junction marker ZO-1 (Fig. 2C) showed two lumenized and perfusable tubules, with separated access to their apical and basal sides. The placental barrier co-cultures were highly reproducible across the platform (Fig. 2D). During gestation, placental barrier thickness is known to decrease, lowering to distances ranging between 20 µm and 100 µm in the first trimester of pregnancy [59,60]. The maternal-fetal interface distance of the placental barrier on-a-chip culture was assessed after 9 days of culture by measuring the shortest, longest, and averaged distance between the epithelium and endothelium (Fig. 2E). The maternal-fetal interface distance ranged below 20 µm up to 130 µm in 75% of the cultures, with 25% below 55 µm. The longest distance and average distance obtained ranges between 51-229 µm and 9–187 µm, respectively for 75% of the cultures. Those variable distances are comparable to the first-trimester *in vivo* situation.

3.2. Trophoblasts differentiate into a polarized syncytium with endocrine functions

In vivo, the syncytium is a polarized and secretory epithelium that is essential for the establishment and maintenance of pregnancy [61]. Those features were confirmed in the placental barrier on-a-chip through gene and protein expression analysis. As shown by positive immunostaining for microvilli marker ezrin (Fig. 3Ai) of the maternal compartment at 9 days of culture, the differentiated trophoblasts expressed microvillar proteins. The 3D reconstruction (Fig. 3Aii) of actin and ezrin staining, showed the formation of a confluent trophoblast layer with microvilli exclusively formed on the apical/luminal side of the epithelium. Syncytium formation was further confirmed at the gene expression level (Fig. 3B). After 48 h of differentiation, BeWo b30 showed an up-regulation of syncytin-2 mRNA, a fusogenic marker involved in trophoblast fusion [62]. It was accompanied by an increase in hCG-α and hCG-ß gene expression, two sub-units of the human chorionic gonadotropin hormone, as well as PlGF, a placental growth factor. At the protein level, a staining of the epithelium for zona

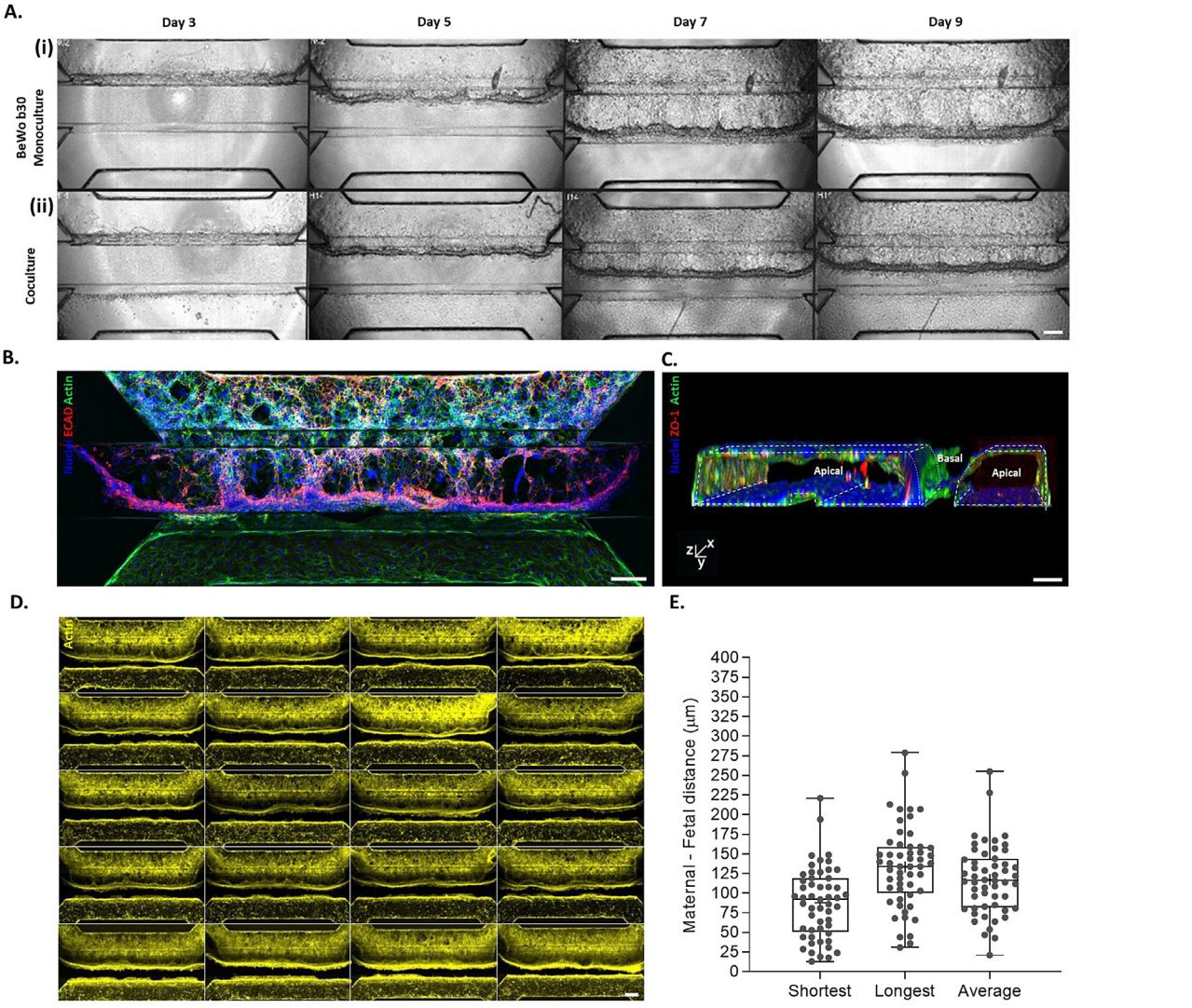

Fig. 2. ECM thickness mimics the physiological placental barrier interface in the early stage of pregnancy. (A) Representative phase contrast images of (i) BeWo b30 monoculture (maternal compartment), or (ii) co-culture with HUVEC (fetal compartment) depicting cell culture growth from day 3 to day 9. Middle channel contains a collagen-I/IV ECM gel. Scale bar: 200 µm. (B) Maximum intensity z-projection of the placental barrier co-culture after 9 days of culture. Staining for Actin (green) and DNA (blue) shows the maternal-fetal interface, with the distinct maternal compartment stained for ECAD (red). Scale bar: 200 µm. (C) 3-dimensionnal reconstruction of the placental barrier stained for ZO-1 (red), Actin (green) and DNA (blue) showing a lumenized maternal and fetal compartment in close proximity. Scale bar: 100 µm. (D) View of 20 chips containing placental barrier cultures after 9 days of culture, stained for Actin (yellow). Scale bar: 100 µm. (E) Maternal-fetal interface distance quantification obtained from placental barrier Actin immunostaining. For every chip, the shortest, longest, and average interface distance between mother and fetal compartment was measured. Data are plotted as box and whiskers ($N = 3$, $n = 16–19$). The line and plus sign represent the median and mean, respectively.

occludence-1 tight junctions (ZO-1) and DNA labeling showed a breakdown of junctions upon differentiation (Fig. 3C) with the formation of a mixed population of cytotrophoblats, multinucleated syncytiotrophoblasts and trophoblasts undergoing fusion (Figure S3). As visualized by Actin staining, trophoblast layer confluency was mainted upon differentiation. Moreover, a staining for hCG-ß and ECAD (Figure 3Di), as well as hCG-ß intensity quantification (Fig. 3E) showed a significant increase of the hormone in the model, which was specifically produced within the syncytiotrophoblasts (Fig. 3Dii). Additionally, while the hormone secretion in the lumen of the maternal compartment (Fig. 3F) remained low and stable overtime (ranging between 497.2 ± 102.1 pg/mL and 1005.1 ± 307.9 pg/mL) in the undifferentiated culture, a significant time-dependent increase was observed upon differentiation, with a 4.5-fold (2145.7 ± 307.9pg/mL) and 12.1-fold increase (5825.9 ± 664.5pg/mL) (Fig. 3G), after 24 h and 48 h differentiation respectively, compared to the undifferentiated epithelium.

3.3. Placental barrier on-a-chip is suitable for paracellular and drug transport studies

In order to provide a tool for transport assessment across the maternal-fetal interface, the placental barrier on-a-chip model was characterized for basement membrane production, crucial for solute filtration, as well as for barrier integrity and drug transport activity. To verify the molecular composition of the basement membrane, syncytium and endothelium were stained for diverse basement membrane proteins (Fig. 4A). Both maternal and fetal compartments secreted laminin and perlecan (Figure 4Ai), collagen-IV (Figure 4Aii) and nidogen-2 (Figure 4Aiii). In contrast, only the endothelium produced fibronectin (Figure 4Aii), while tenascin-C was solely secreted by the syncytium (Figure 4Aiii). The syncytium constitutes the main physical barrier for paracellular transport of solutes [60]. To characterize syncytium barrier tightness in our model, a fluorescent 4.4 kDa TRITC-labelled dextran was administrated to the lumen of the trophoblast tubule (Fig. 4B). Leak-

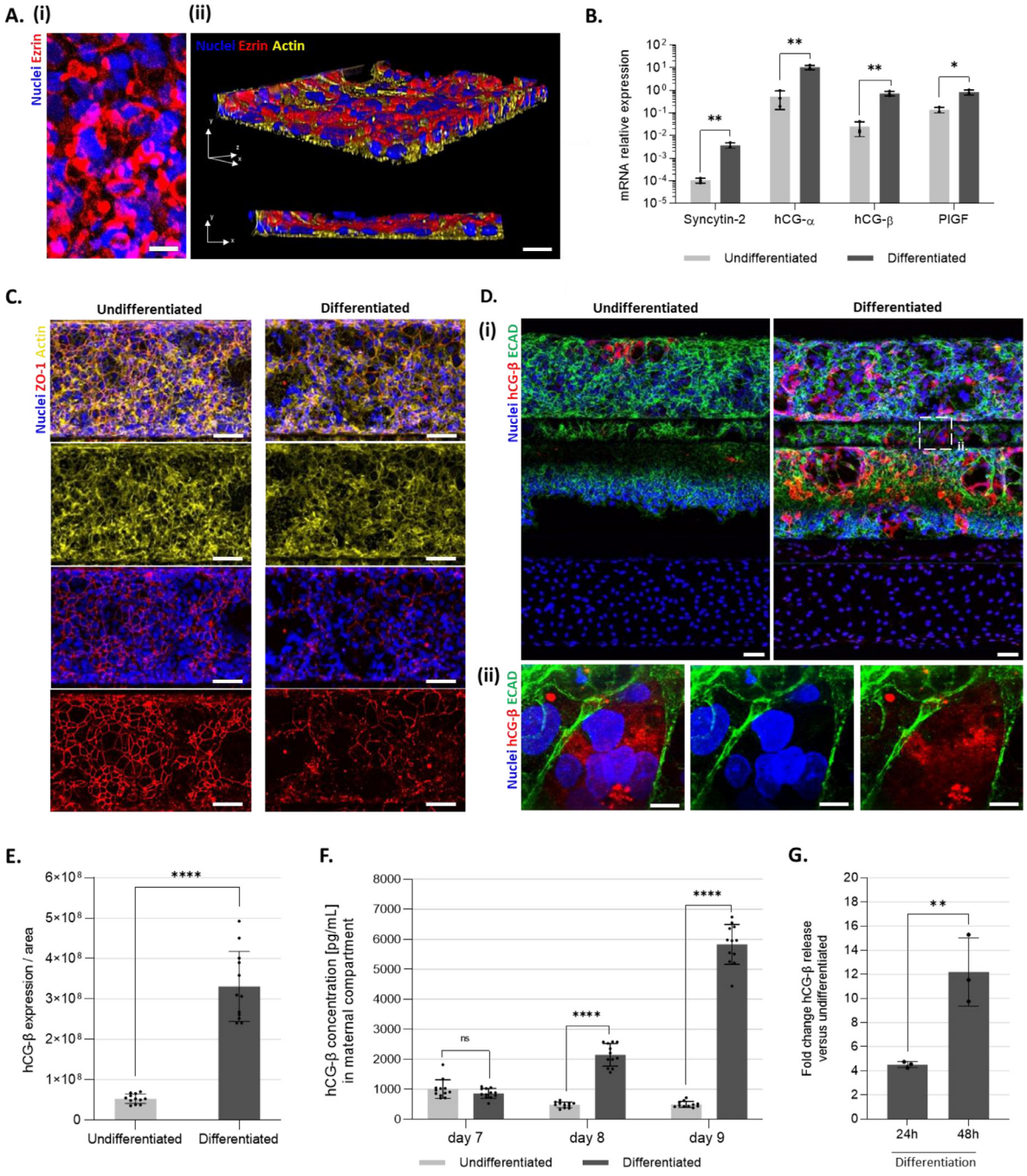

Fig. 3. Trophoblasts differentiate into a polarized syncytium. (A) (i) Representative maximum intensity z-projection of syncytium microvilli stained for Ezrin (red) and DNA (blue). Scale bar: 25 µm. (ii) 3-dimensional reconstruction of the syncytium layer stained for Ezrin (red), Actin (yellow) and DNA (blue) shows a polarized syncytium. Scale bar: 50 µm (B) mRNA expression of trophoblast differentiation markers Syncytin-2, hCG-α, hCG-ß and PlGF in undifferentiated or differentiated BeWo b30 (48 h 25 µM Forskolin + 10 nM PMA+ 10 µM MMP-8 inhibitor). Each data point is derived from 5 pooled chips. Graphs show the mean of relative expression values normalized to GAPDH ± SEM and statistical analysis was performed using a one-way ANOVA ($N = 1$, $n = 3$). (C) Representative maximum intensity z-projection of undifferentiated and differentiated BeWo b30 stained for ZO-1 (red), Actin (yellow) and DNA (blue) shows the formation of multinucleated syncytium upon differentiation. Scale bar: 100 µm (D) Representative and (i) maximum intensity z-projection of undifferentiated and differentiated BeWo b30 stained for ECAD (green), hCG-ß (red) and DNA (blue). Scale bar: 100 µm. A zoom-in (ii) shows trophoblast hormone production within the formed syncytium. Scale bar: 20 µm. (E) Fluorescence intensity analysis of SUM projections of hCG-ß immunostaining from undifferentiated or differentiated BeWo b30. The intensity is corrected for the isotype control. Data points represent individual chips. Data was presented as mean ± standard deviation (SD) and statistical analysis was performed using two-tailed unpaired *t*-test ($N = 3$, $n = 4$). (F) Apical secretion of hCG-ß from undifferentiated and differentiated epithelium at day 7 (before differentiation), day 8 (24 h differentiation) and day 9 (48 h differentiation). Data points represent individual chips. Data was presented as mean ± SD and statistical analysis was performed using ordinary two-way ANOVA ($N = 3$, $n = 4$). (G) Fold change of hCG-ß release in the lumen of differentiated over undifferentiated BeWo b30 at day 8 (24 h differentiation) and day 9 (48 h differentiation). Data points represent the average of hCG-β concentration of differentiated over undifferentiated epithelium of 4 chips. Data was acquired from 3 individual experiments. Data were presented as mean ± SD and statistical analysis was performed using two-tailed unpaired *t*-test ($N = 3$, $n = 4$). ns: non-significant; * $P < 0.05$; ** $P < 0.01$; **** $P < 0.0001$.

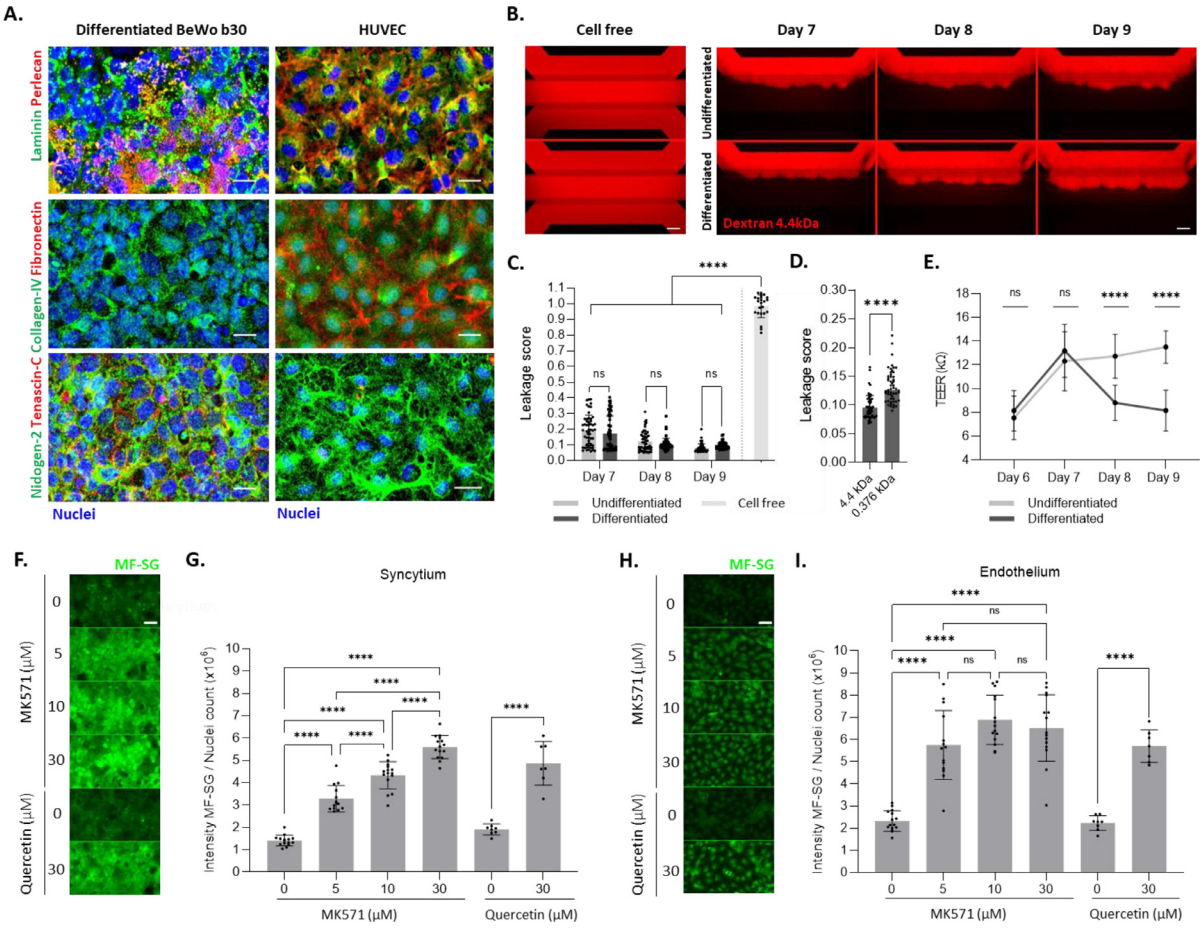

Fig. 4. Placenta on-a-chip forms a leaktight barrier and is suitable for drug transport studies. (A) Representative maximum intensity z-projection of syncytium and endothelium stained for DNA (blue) and the basement membrane proteins (i) laminin (green) and perlecan (red), (ii) collagen-IV (green) and fibronectin (red), (iii) nidogen-2 (green) and tenascin-C (red). Scale bar: 25 μm (B) Fluorescent images of representative undifferentiated and differentiated placental barrier co-culture, perfused in the maternal compartment with fluorescent molecules (red) using 4.4 kDa TRITC-Dextran for 12 min on days 7, 8 and 9. Scale bar: 100 μm Trophoblast differentiation was started on day 7 in the Differentiated condition. The cell free control showed passage of the fluorescent dye into the adjacent gel and perfusion channel, whereas fluorescent dye was retained by undifferentiated and differentiated trophoblast tubules. (C) Ratio of 4.4 kDa TRITC-Dextran intensity in the basal side of the maternal tube *versus* the intensity at the apical side of the maternal tube (Leakage score) after $T = 12$ min, on days 7, 8 and 9. Data points represent individual chips. Data are presented as mean ± SD and statistical analysis was performed using ordinary two-way ANOVA ($N = 3$, $n = 17–19$ for undifferentiated and differentiated conditions; $N = 3$, $n = 6–9$ for cell free) (D) Ratio of 4.4 kDa TRITC-Dextran and Fluorescein (0.376 kDa) intensity in the basal side of the maternal tube *versus* the intensity at the apical side of the maternal tube (Leakage score) in differentiated trophoblasts at 9 days of culture after $T = 12$ min. Data are presented as mean ± SD and statistical analysis was performed using two-tailed unpaired *t*-test ($N = 3$, $n = 17–18$). (E) Transepithelial electrical resistance (TEER) measured on undifferentiated and differentiated trophoblasts on days 6, 7, 8 and 9. Trophoblast differentiation was started on day 7 in the Differentiated condition. Data is presented as mean ± SD and statistical analysis was performed using ordinary two-way ANOVA ($N = 3$, $n = 9–21$). (F)-(I) Evaluation of Multi-Drug Resistance Protein (MRP) transporter activity in the placental barrier on-a-chip. The non-fluorescent CMFDA was used as MRP substrate. It enters the cells passively and transforms inside the cells into its fluorescent product MF-SG. (F) & (H) Representative summary z-projections of intracellular GS-MF (green) intensity in differentiated trophoblasts (F) and endothelium (H) treated for 30 min with vehicle (DMSO) or two MRP specific inhibitors, MK571 (5 μM, 10 μM, 30 μM) and quercetin (30 μM). Scale bar: 50 μm (G) & (I) Ratio of GS-MF intensity over nuclei count in the syncytium (G) and endothelium (I). A dose-dependent inhibition of MRP transporters by MK571 and Quercetin is observed. Data points represent individual chips. Data are presented as mean ± SD and statistical analysis was performed using ordinary one-way ANOVA ($N = 3$, $n = 4$ for MK571; $N = 2$, $n = 4$ for Quercetin). ns: non-significant; **** $P < 0.0001$.

age from the lumen to the adjacent gel compartment was monitored for undifferentiated and differentiated trophoblast tubules at 7, 8 and 9 days of culture. Both undifferentiated and differentiated epithelium formed a leak-tight barrier that was stable over time, showing low and non-significant leakage scores ranging from 0.19±0.10 and 0.17±0.11 on day 7 to 0.08±0.03 and 0.10±0.02 on day 9, for undifferentiated and differentiated epithelium, respectively (Fig. 4C). In the same manner, fluorescein (0.376 kDa) transfer across the trophoblast barrier was assessed from days 7 to 9 (Figure S4). At 9 days of culture, fluorescein paracellular transport (0.10±0.02 leakage score) was increased by 38.5% compared to 4.4 kDa TRITC-labelled Dextran (0.13±0.03 leakage score) (Fig. 4D). The transepithelial electrical resistance (TEER) (Fig. 4E) revealed that an undifferentiated epithelial barrier increased its tightness over time with TEER values ranging from 7.56±1.83 kΩ on day 6 to 13.50±1.35 kΩ on day 9, whereas trophoblast epithelium showed a time-dependent decrease upon differentiation with TEER values dropping from 13.19±2.24 kΩ on day 7 to 8.17±1.71 kΩ on day 9.

Throughout pregnancy, drug transporters in the placenta protect the fetus from xenobiotics [63]. We therefore demonstrated the functionality of the multi-drug resistance protein (MRP) family in our placenta model. The model expressed MRP1, MRP2, MRP5 and less abundantly MRP3 and MRP4 at the mRNA level (Figure S5). The cell tracker 5-chloromethylfluorescein diacetate (CMFDA) and its fluorescent metabolite MF-SG are well-known MRP substrates [64]. MRP-mediated transport was assessed on day 9 of culture in the syncytium and endothelium using MK571 and quercetin, two MRP inhibitors. In presence of MK571 and quercetin in both maternal (Fig. 4F, G) and fetal (Fig. 4H, I) compartments, there was a dose-dependent increase in the intracellular fluores-

cence intensity indicating the inhibition of MRP-mediated efflux transport in both syncytium and endothelium. In a similar set up, the Breast Cancer Resistance Protein (BCRP), which restricts the distribution of its substrates to the fetus, was shown to be active in the syncytium of the placental barrier-on-a-chip setup (Fig. S6).

4.4. Impaired oxygen tension and perfusion induces molecular and functional changes in the placental barrier that closely resembles those observed in pathologies associated with uteroplacental hypoxia

Hypoxia and ischemia are central mechanisms of damage to the placenta leading to induction of preeclampsia (PE), intrauterine growth restriction (IUGR) and gestational hypertension [65]. In order to model features associated with uteroplacental hypoxia pathologies in the placental barrier on-a-chip model, cultures were exposed to a combination of different oxygen and perfusion tensions. Parameters to mimic healthy conditions included 20% O_2 and perfusion flow and are here referred to as the "Normoxic" condition (Figure 5Ai). Diseased environment was mimicked by either switching the culture to 1% O_2 with medium perfusion flow for 24 h on day 8 ("Hypoxic") or to 1% O_2 and static medium conditions ("Ischemic"). Oxygen levels within the placental barrier models were monitored in the different culture set-ups with oxygen sensors (Figure S7A). Oxygen levels in placental barrier cultures showed a significant drop 1 h after being exposed to hypoxic and ischemic environement and reached an oxygen level equivalent to 1% O_2 5–6 h later (Figures S7B-D). Phase contrast images of the placental barriers cultured under different oxygen tensions and perfusion rates did not show a change in culture growth and stability (Fig. 5B). However, measurement of transepithelial electrical resistance (TEER) through the syncytia (Fig. 5C) on day 8 and day 9 revealed that the "Ischemic" environment triggers syncytium integrity damage. Indeed, while both "Normoxic" and "Hypoxic" conditions showed respectively a 1.23 and 1.29-fold decrease in TEER values over time, indicating hypoxia itself did not affect the epithelium barrier, the "Ischemic" condition triggered a significant 1.9-fold change decrease in syncytium permeability. Interestingly, nuclei count over a representative syncytium area (Figure S8A) showed 10% more cells in the "Ischemic" condition (Fig. 5D, E) compared to the "Normoxic" condition, an increase which was not observed in the "Hypoxic" condition. While hypoxia did not significantly affect cell viability, the ischemic set-up led to an increase in cell death, in both syncytium and endothelium (Figure S9).

The different syncytia were then characterized at the gene expression level (Fig. 5F) for markers known to be mis-regulated in placenta pathologies. In comparison to the "Normoxic" model, the fusogenic marker, syncytin-2 exhibited a 1.58-fold decrease in the "Hypoxic" and 0.58-fold change decrease in the "Ischemic" conditions. Likewise, the mRNA level of two human chorionic gonatropin isoforms hCG-α and hCG-β were downregulated to a greater extent in "Hypoxic" with a 1.52-fold change and 2.13-fold change respectively, compared to 1.04-fold change and 1.57-fold change for "Ischemic" conditions. Finally, placental growth factor PlGF, a predictive biomarker of preeclampsia [66] also showed a decrease in expression under low oxygen tension with a 1.81-fold change decrease, while it was reduced to a 1.48-fold change after exposure to hypoxia-ischemia environment.

The syncytium was further characterized at the protein level. Immunostaining for the microvilli marker, Ezrin (Fig. 5G) showed a modest increase in the "Hypoxic" condition compared to the "Normoxic" placenta model that was not statistically significant (Fig. 5H). However, the "Ischemic" condition exhibited 50% lower expression of Ezrin than the "Normoxic" placenta model. Moreover, patched loss of Ezrin signal in the "Ischemic" condition showed a complete loss of microvilli in those cell surface areas (Figure S8B). Compared to the "Normoxic" condition, the signal for hCG-β (Fig. 5I, J) was decreased for the "Hypoxic" condition, which was amplified to 25% for the "Ischemic" condition. This reduction in hCG-β was confirmed at the secretion level by measuring the hormone release into the syncytium lumen (Fig. 5K) before and after 24 h exposure to the different oxygen/perfusion environments. Indeed, while the hormone showed a 3.06-fold increase in secretion in the "Normoxic" placenta model, only a 1.84-fold and 1.67-fold increase was observed in "Hypoxic" and "Ischemic" respectively. Additionally, glucose transporter-1 (GLUT-1), a major regulatory factor in the process of maternal-fetal glucose exchange was evaluated at the protein level expression (Figure S10) and demonstrated to decrease 25% after 24 h culture under "Ischemic" conditions compared to the control. Taken together, these data showed that hypoxia itself or combined with static conditions could induce phenotypical changes in our placental barrier co-culture.

4. Discussion

In this study, we report the *in vitro* modeling of uteroplacental hypoxia associated disease characteristics in the form of a placental barrier on-a-chip in a multi-parallel setup. The healthy placental barrier model recapitulated essential features of early pregnancy, such as barrier formation, polarization, transporter function and hormone secretion. Exposure of the placental barrier model to an ischemic and hypoxic environment triggered alterations in syncytium integrity and functionality at different degrees, representative of syncytial alterations linked to placental pathologies, such as preeclampsia (PE).

Progressing with days in culture, BeWo b30 exhibited invasive behavior (Fig. 2) likely supported by the secretion of a wide range of metalloproteinases (MMPs) [43] and characteristics of their malignant properties. *In vivo*, trophoblast-matrix remodeling is regulated via the secretion of a wide range of metalloproteinases and their inhibitors [67,68]. While MMP regulation has not been studied in this model, investigation of matrix metalloproteinases expression and secretion, as well as their effect on cell morphology and collagen organization, would give more insights on BeWo invasive behavior and how it compares to the *in vivo* situation. Because the placental barrier ECM gel was mainly composed of collagen-I [44], MMP-8 inhibitor was used to control BeWo b30 invasion. Additionally, fetal endothelium proved important for the stabilization of the materno-fetal distance. The placental barrier interface distance reached distances below 20 µm, with variations within the same chip, which is in line with studies reporting an irregular maternal-fetal diffusion distance of 10–100 µm in the first trimester of pregnancy *in vivo* [60,69]. In the literature, trophoblast cells are often compared to malignant cells because of their invasive behavior [67]. Even though their degree of ECM degradation and migration might differ from BeWo b30, they present strong similarities in the mechanisms involved [70]. Thus, the co-culture set-up of ECM, BeWo b30 and HUVEC in a membrane-free manner provides a unique advantage for modeling this progressive thinning of the maternal interface that would not be present for membrane-based systems such as Transwell or microfluidics devices that make use of artificial membranes [27,28].

In vivo, Ezrin is linking the microvillar F-actin core to the membrane of syncytiotrophoblasts and constitutes an essential component of the morphogenesis of their apical domain [71–73]. Characterization of the differentiated syncytia for Ezrin over Actin staining (Figure 3) showed Ezrin apical localization, demonstrating the establishment of apicobasal polarization. Microvilli pointed out towards the maternal compartment lumen, reflecting the *in vivo* syncytium with an extensive microvillous brush barrier in contact with the maternal blood [74]. These microvilli are essential to increase the available surface area for material exchange and transporter polarization [75,76]. The 48 h differentiation of BeWo b30

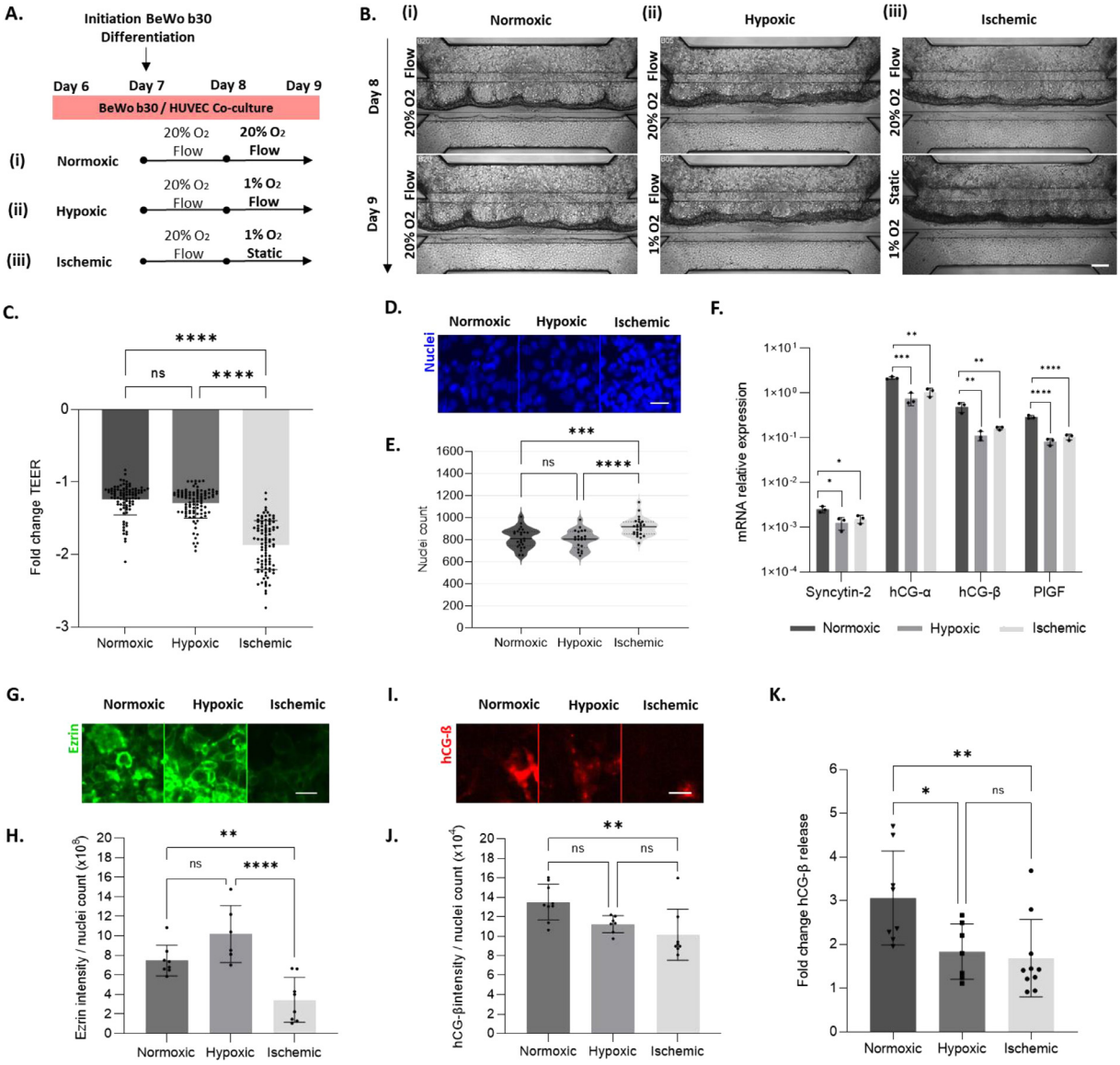

Fig. 5. Low oxygen tension and lack of perfusion result in syncytium damage resembling preeclamptic characteristics (A) Workflow depicting the parameters to mimic healthy and preeclamptic conditions. On day 8, the placental barrier model is either (i) kept under standard condition: 20% O_2 and flow ("Normoxic"), (ii) cultured for 24 h under 1% O_2 and flow ("Hypoxic") or (iii) cultured for 24 h under 1% O_2 and static ("Ischemic"). (B) Representative phase contrast images of the placental barrier on-a-chip model depicting (i) "Normoxic", (ii) "Hypoxic" and (iii) "Ischemic" conditions over 8 and 9 days of culture. Scale bar: 200 µm. (C) Fold change decrease of transepithelial electrical resistance (TEER) values of the syncytium on day 9 *versus* day 8 in "Normoxic", "Hypoxic" and "Ischemic" conditions. Data points represent individual chips. Data are presented as mean ± SD and statistical analysis was performed using ordinary one-way ANOVA ($N = 3$, $n = 30–33$). (D) Representative summary z-projections of syncytium nuclei count in "Normoxic", "Hypoxic" and "Ischemic" conditions after 9 days of culture. Scale bar: 50 µm. (E) Quantification of the nuclei count in "Normoxic", "Hypoxic" and "Ischemic". Data points represent individual chips. Data points are represented as dispersion, with the average (solid line) ± SD (dotted line) and statistical analysis was performed using ordinary one-way ANOVA. ($N = 3$, $n = 21–25$). (F) mRNA expression of trophoblast differentiation markers Syncytin-2, hCG-α, hCG-ß and PlGF in "Normoxic", "Hypoxic" and "Ischemic". Each data point is derived from 5 pooled chips. Graphs show mean of relative expression values normalized to Actin ± SEM and statistical analysis was performed using ordinary one-way ANOVA ($N = 1$, $n = 3$). (G) Representative summary z-projections of Ezrin intensity in "Normoxic", "Hypoxic" and "Ischemic" conditions. Scale bar: 50 µm. (H) Ratio of Ezrin intensity over nuclei count of the syncytium, in "Normoxic", "Hypoxic" and "Ischemic" conditions. Data points represent individual chips. Data are presented as average signal intensity / nuclei count ± SD and statistical analysis was performed using ordinary one-way ANOVA ($N = 2–3$, $n = 2–3$). (I) Representative summary z-projections of hCG-ß intensity in "Normoxic", "Hypoxic" and "Ischemic" conditions. Scale bar: 50 µm. (J) Ratio of hCG-ß intensity over nuclei count in the syncytium, in "Normoxic", "Hypoxic" and "Ischemic" conditions. Data points represent individual chips. Data are presented as mean ± SD and statistical analysis was performed using ordinary one-way ANOVA ($N = 3$, $n = 2–3$). (K) Fold change increase of apical secretion of hCG-ß into the maternal compartment lumen in "Normoxic", "Hypoxic" and "Ischemic" conditions on day 9 *versus* day 8. Data points represent individual chips. Data are represented as mean ± SD and statistical analysis was performed using ordinary two-way ANOVA ($N = 3$, $n = 3–4$). ns: non-significant, * $P < 0.05$; ** $P < 0.01$; *** $P < 0.001$; **** $P < 0.0001$).

resulted in a significant up-regulation of syncytin-2, a gene playing a critical role in the fusion of trophoblasts [42]. It was translated at the molecular level by a loss of ZO-1 tight junctions, leading to the formation of an epithelium consisting of a mixed population of trophoblasts and multinucleated syncytiotrophoblasts (Figure S3). Syncytium formation, in our model as in placenta from pregnant women, is a transient process making trophoblast cell subpopulation quantification, and thus their comparison with *in vivo* placenta, challenging. However, the continuous syncytium, trophoblasts displaying morphological appearance between undifferentiated state and syncytiotrophoblasts, as well as decreased but apparent pool of mononucleated trophoblasts in our model is characteristics of gestational placenta with auto-regenerative syncytium layer properties [10]. Up-regulation of hCG subunits was

confirmed at the mRNA level and hCG-ß production was significantly increased and secreted into the maternal compartment. These data are in agreement with previous studies in BeWo cell lines reporting elevated hormone release upon chemical stimulation with Forskolin [77,78]. *In vivo*, hCG-ß is regarded as one of the main markers of differentiation and its increased production in the first months of gestation is critical for the maintenance of early pregnancy [42]. Finally, syncytium formation was associated with an elevation of placental growth factor (PlGF) mRNA, a proangiogenic factor known to mainly be produced by syncytiotrophoblasts with the role to promote placental angiogenesis during pregnancy [79]. Taken together, these data confirmed a successful syncytium development in the placental barrier co-culture.

On their basal sides, the syncytium and endothelium successfully secreted their own basal lamina as observed by the production of laminin, heparan sulfate (perlecan), collagen-IV and nidogen-2 (Fig. 4). The trophoblasts also expressed tenascin-C, a matrix protein involved in syncytial fusion and playing a critical role in placental homeostasis development [80]. Syncytium did not secrete fibronectin, which may contribute to their malignant origin [81]. Those secreted proteins are well known to act both as functional support and as a filtration barrier between the maternal-fetal interface [82]. Assessment of the paracellular flux of two different molecular-weight solutes across the maternal barrier demonstrated the formation of a leaktight syncytium for 4.4 kDa molecules (Fig. 4C), with a higher permeability to fluorescein (0.376 kDa) (Fig. 4D) increasing upon differentiation (Figure S4). Those results corroborate those previously reported, demonstrating a size-dependent passive diffusion of molecules across BeWo cells and primary trophoblasts *in vitro* [83] and a passive diffusion of drugs <500 Da across the syncytium *in vivo* [59]. Similarly, the absolute TEER (Ω) values, calculated to discriminate the impact of epithelium changing surface upon differentiation, showed a decrease upon syncytium formation (Fig. 4E). Stimulation of BeWo cells with cAMP activator in 2D has been shown to lead to the formation of large openings, as a result of trophoblast fusion, making them unusable for transport studies [83]. The use of undifferentiated trophoblasts in current placental barrier on-a-chip models [27,29–34] is likely linked to this particularity. However, our setup allowed direct culture of cells against ECM and thus remodeling of the matrix, which enabled the formation of a leaktight differentiated syncytium.

Additionally, the placental barrier on-a-chip presents active MRP and BCRP drug transporters. The combination of CMFDA substrate with MK175 or quercetin suggested that MRP1/2, transporter subtypes present in cytotrophoblasts and syncytiotrophoblasts of first trimester placenta [84], were active [59,85]. We thus effectively developed *in vivo*-like features making our placental barrier on-a-chip a relevant tool for transplacental transport studies.

Insufficient uteroplacental oxygenation together with ischemia is considered to be among the leading causes of uteroplacental pathologies [86]. We mimicked different development environments by exposing the placental barrier-on-a-chip to 1% O_2 level, either under perfusion ("Hypoxic") or static ("Ischemic") conditions, for 24 h (Fig. 5). While hypoxia itself did not cause syncytium barrier disruption, removal of perfusion flow resulted in a significant increase of permeability which was associated with a loss of syncytial microvilli. Those results are in line with studies showing that induced-hypoxia in static BeWo b30 cultures was accompanied by defective paracellular transport through alteration of tight-junctions [87]. While there is limited *in vivo* data available regarding syncytium permeability during PE, the pathology is known to be associated with syncytial degeneration, damaged syncytium integrity and loss of microvilli [36,88], strongly suggesting alteration in syncytium permeability [89]. Syncytium damage observed under ischemia was likely triggered by a loss of flow, reducing diffusion of nutrients and removal of waste in the placental barrier on-a-chip. Interestingly, the *in vitro* "Ischemic" model showed an increase in the trophoblast cell population as well as an increase in cell death. This is in line with *in vivo* studies in placenta issued from normal and preeclamptic pregnancies revealing a higher proliferation rate of villous trophoblast in the diseased placenta [90,91] as well as excessive trophoblast cell death [92]. While some designated these excessive proliferative cells as immature and intermediate trophoblasts [91], others stipulated that this higher proliferation rate is a mechanism to counteract syncytium damage [36]. In order to get more insights into the state of the trophoblasts in our diseased models, mechanisms involved in cell proliferation and cell death, such as apoptosis and necrosis, will be further investigated. A down-regulation of markers involved in syncytium differentiation, such as Syncytin-2, hCG-α, hCG-ß, was observed at the gene expression level in both preeclamptic models. The loss of syncytin-2 is in line with earlier studies showing that PE-mimicking hypoxia in BeWo b30 and primary trophoblast cells [93,94] or cells isolated from PE placentas [95] presented reduced cell fusion. Moreover, another study stipulated that syncytin downregulation correlates with the severity of PE, and can serve as a marker to evaluate women at risk of developing PE during pregnancy [96]. Regarding hCG-ß, the downregulation at the gene expression level was translated at the molecular level by a reduced hormone production and secretion into the maternal compartment, with a more pronounced effect when low oxygen tension was combined with the static condition (Fig. 5K). This correlates with the evidence that low hCG-ß concentrations late in the first trimester may be associated with a subsequent risk of preeclampsia [97]. Also, low PlGF expression and concentration observed in preeclampsia, a biomarker of PE pathology [66], was replicated at the mRNA level in our "Hypoxic" and "Ischemic" models. While we focused here on the alterations of the syncytium, this model would provide a good tool to study the effect of change in oxygen tension and perfusion on the expression of basement membrane proteins, such as laminin, which are known to be altered during PE [98].

The trophoblast cell line used in our model has been widely used in placental research. It has been reported to display several morphological properties and functions common to primary trophoblasts, such as differentiation into syncytiotrophoblasts, hormones production and polarized transcellular transports [99]. However, due to their choriocarcinoma origin, they do not differentiate spontaneously *in vitro* [100] and show different methylation patterns compared to primary trophoblasts, contributing to variation in the expression of numerous genes, implying that care must be taken when extrapolating results [101]. While differences are observed in placental drug transporter expression [102], further studies assessing transplacental transfer of drugs by mass spectrometry would increase insight in transport capabilities of our model. The feasibility of conducting LC-MS studies in the OrganoPlate have already been proven successful [103], guaranteeing its applicability to the placental barrier on-a-chip. In the past year, tremendous efforts have been conducted in the development of more physiologically relevant alternatives with the generation of cytotrophoblast stem-like cells from hPSCs [104,105] or long-term trophoblast organoids [106]. Their integration into our platform would move the placental barrier on-a-chip a step further in the modeling and study of normal and diseased placenta in early pregnancy [104]. Regarding the oxygen tension used in the co-culture set-up, the 20% O_2 level differs from the hypoxic placental environment which reaches up to 6–8% at the end of the first trimester [9]. However, we choose to adhere to common practice to culture in a 20% O_2 environment, as this is more practical for long-term culture, avoids oxygen adjustments and allows us to compare our results with data from the literature. For disease modeling, we exposed both the maternal and fetal compartments to hypoxic (1%

O_2) and ischemic (1% O_2, static) environments to mimic placental and fetal hypoxia. Applying an oxygen gradient to the culture set-up to initiate hypoxia in the maternal compartment only would be interesting to study the progression of the disease.

Lastly, uteroplacental pathologies associated with impaired remodeling of spiral arteries are characterized by an intermittent maternal blood flow within the intervillous space associated with ischemia/hypoxia – reperfusion type of injury. While we only focused on the hypoxic and ischemic/hypoxic aspects, reperfusion modeling would be of a great interest, especially for the study of oxidative stress and release of anti-angiogenic factors, which are other hallmarks of PE [107].

5. Conclusion

We described here the first placental barrier on-a-chip system modeling pathological characteristics linked to uteroplacental hypoxia. The model recapitulates key features of the placental barrier in early pregnancy such as syncytium differentiation, barrier function, polarization, hormone secretion and transporter abilities. In addition, by recreating a hypoxic/ischemic environment, we could effectively recapitulate some phenotypical characteristics observed in preeclampsia, such as reduced barrier function, hormonal secretion, brush border formation and increased nuclei count. The healthy model represents a powerful tool for modeling drug placental transfer assessment during pregnancy. Exposure to hypoxic and ischemic conditions will prove beneficial to improve our understanding of uteroplacental pathologies. Its potential for high-throughput screening approaches will open tremendous opportunities in the identification of new targets and the development of therapies for the prevention or treatment of those diseases.

Author contributions

G. Rabussier, H.L. Lanz and K. Bircsak conceptualized the study. G. Rabussier, I. Bünter, T. van Zijp and J. Bouwhuis performed the investigation, data curation and formal analysis. H.L. Lanz, K. Bircsak, K. Domansky, C.E. Mudoch and L.J. de Windt supervised the research. G. Rabussier, H.L. Lanz and K. Bircsak wrote the paper. G. Rabussier, C. Soragni, C. Ping Ng, H.L. Lanz and K. Bircsak contributed to the visualization. All authors read and approved the final manuscript.

Disclosures

G. Rabussier, I.Bünter, J. Bouwhuis, C. Soragni, T. van Zijp, C. Ping Ng, K. Domansky, P. Vulto, K. Bircsak and H.L. Lanz are or were employees of MIMETAS BV, The Netherlands, which is marketing the OrganoPlate. P. Vulto is shareholder of the same company. OrganoPlate, OrganoTEER and OrganoFlow are trademarks of MIMETAS BV.

Declaration of Competing Interest

The authors declare that they have no known competing financial interests or personal relationships that could have appeared to influence the work reported in this paper.

Acknowledgements

This work was supported by the European Union's Horizon 2020 research and innovation program iPlacenta under grant agreement No. 765274. Graphical abstract and Fig. 1c have been created with BioRender.com. We would like to acknowledge Frederik Schavemaker for the artwork and Ryan Titmas, Nick Quan, Richard Bryan and Walker Inman from Lucid Scientific for their support in the oxygen measurements with their Resipher device.

Supplementary materials

Supplementary material associated with this article can be found, in the online version, at doi:10.1016/j.actbio.2023.04.033.

References

[1] D. Hutter, J. Kingdom, E. Jaeggi, Causes and mechanisms of intrauterine hypoxia and its impact on the fetal cardiovascular system: a review, Int. J. Pediatr 2010 (2010) 1–9, doi:10.1155/2010/401323.
[2] D. Sharma, S. Shastri, P. Sharma, Intrauterine growth restriction: antenatal and postnatal aspects, Clin. Med. Insights Pediatr. 10 (2016) CMPed.S40070, doi:10.4137/cmped.s40070.
[3] L. Duley, The global impact of pre-eclampsia and eclampsia, YSPER 33 (2009) 130–137, doi:10.1053/j.semperi.2009.02.010.
[4] L. Say, D. Chou, A. Gemmill, Ö. Tunçalp, A.B. Moller, J. Daniels, A.M. Gülmezoglu, M. Temmerman, L. Alkema, Global causes of maternal death: a WHO systematic analysis, Lancet Glob. Heal. 2 (2014) 1–11, doi:10.1016/S2214-109X(14)70227-X.
[5] G. Hypertension, ACOG Practice Bulletin No. 202: gestational hypertension and preeclampsia, Obstet. Gynecol. 133 (2019) e1–e25, doi:10.1097/AOG.0000000000003018.
[6] H. Al-Jameil, N. Aziz Khan, F. Fareed Khan, M. Tabassum, A brief overview of preeclampsia, J. Clin. Med. Res. 6 (2013), doi:10.4021/jocmr1682w.
[7] K.A. Pennington, J.M. Schlitt, D.L. Jackson, L.C. Schulz, D.J. Schust, Preeclampsia: multiple approaches for a multifactorial disease, DMM Dis. Model. Mech. 5 (2012) 9–18, doi:10.1242/dmm.008516.
[8] A. Wang, S. Rana, S.A. Karumanchi, Preeclampsia: the role of angiogenic factors in its pathogenesis, Physiology 24 (2009) 147–158, doi:10.1152/physiol.00043.2008.
[9] N.M. Gude, C.T. Roberts, B. Kalionis, R.G. King, Growth and function of the normal human placenta, Thromb. Res. 114 (2004) 397–407, doi:10.1016/j.thromres.2004.06.038.
[10] B. Huppertz, The anatomy of the normal placenta, J. Clin. Pathol. 61 (2008) 1296–1302, doi:10.1136/jcp.2008.055277.
[11] S.K. Griffiths, J.P. Campbell, Placental structure, function and drug transfer, Contin. Educ. Anaesthesia, Crit. Care Pain. 15 (2015) 84–89, doi:10.1093/bjaceaccp/mku013.
[12] Pevzner, Trophoblast lineage specification, differentiation, and their regulation by oxygen tension, Physiol. Behav. 176 (2017) 139–148, doi:10.1530/JOE-17-0402.
[13] L.W. Leaphart, D.B. Byck, X. Zhu, S. Jiang, Morphological changes of placental syncytium and their implications for the pathogenesis of preeclampsia, Cell. Mol. Life Sci. 73 (2017) 365–376, doi:10.1007/s00018-015-2069-x.
[14] R. Raghupathy, Cytokines as key players in the pathophysiology of preeclampsia, Med. Princ. Pract. 22 (2013) 8–19, doi:10.1159/000354200.
[15] I. Carrasco-Wong, M. Aguilera-Olguín, R. Escalona-Rivano, D.I. Chiarello, L.J. Barragán-Zúñiga, M. Sosa-Macías, C. Galaviz-Hernandez, S. San Martín, J. Gutiérrez, Syncytiotrophoblast stress in early onset preeclampsia: the issues perpetuating the syndrome, Placenta 113 (2021) 57–66, doi:10.1016/j.placenta.2021.05.002.
[16] P. Calis, L. Vojtech, F. Hladik, M.G. Gravett, A review of ex vivo placental perfusion models: an underutilized but promising method to study maternal-fetal interactions, J. Matern. Neonatal Med. 0 (2021) 1–13, doi:10.1080/14767058.2021.2005565.
[17] N. Arumugasaamy, K.D. Rock, C.Y. Kuo, T.L. Bale, J.P. Fisher, Microphysiological systems of the placental barrier, Adv. Drug Deliv. Rev. 161–162 (2020) 161–175, doi:10.1016/j.addr.2020.08.010.
[18] K.L. Gatford, P.H. Andraweera, C.T. Roberts, A.S. Care, Animal models of preeclampsia: causes, consequences, and interventions, Hypertension 75 (2020) 1363–1381, doi:10.1161/HYPERTENSIONAHA.119.14598.
[19] A.H. Katrina Chau, Mikala Welsh, Angela Makris, Progress in preeclampsia: the contribution of animal models, J. Hum. Hypertens. (2021).
[20] M. Cherubini, S. Erickson, K. Haase, Modelling the human placental interface in vitro—a review, Micromachines (2021) 12, doi:10.3390/mi12080884.
[21] W.X. Zhao, X. Zhuang, T.T. Huang, R. Feng, J.H. Lin, Effects of notch2 and notch3 on cell proliferation and apoptosis of trophoblast cell lines, Int. J. Med. Sci. 12 (2015) 867–874, doi:10.7150/IJMS.12935.
[22] S. Tamaru, Y. Mizuno, H. Tochigi, T. Kajihara, Y. Okazaki, R. Okagaki, Y. Kamei, O. Ishihara, A. Itakura, MicroRNA-135b suppresses extravillous trophoblast-derived HTR-8/SVneo cell invasion by directly down regulating CXCL12 under low oxygen conditions, Biochem. Biophys. Res. Commun. 461 (2015) 421–426, doi:10.1016/j.bbrc.2015.04.055.
[23] A.C. Eddy, H. Chapman, E.M. George, Acute hypoxia and chronic ischemia induce differential total changes in placental epigenetic modifications, Reprod. Sci. 26 (2019) 766–773, doi:10.1177/1933719118799193.
[24] V. van Duinen, S.J. Trietsch, J. Joore, P. Vulto, T. Hankemeier, Microfluidic 3D cell culture: from tools to tissue models, Curr. Opin. Biotechnol. 35 (2015) 118–126, doi:10.1016/j.copbio.2015.05.002.
[25] L.A. Low, C. Mummery, B.R. Berridge, C.P. Austin, D.A. Tagle, Organs-on-chips: into the next decade, Nat. Rev. Drug Discov. 20 (2021) 345–361, doi:10.1038/s41573-020-0079-3.
[26] J.H. D.H. Ji Soo Lee, Roberto Romero, Yu Mi Han, Hee Chan Kim, Chong Jai Kim, Placenta-on-a-chip: a novel platform to study the biology of the human

placenta, J. Matern. Fetal Neonatal Med. 29 (2016) 1046–1054, doi:10.3109/14767058.2015.1038518.
[27] B. Mosavati, A.V. Oleinikov, E. Du, Development of an organ-on-a-chip-device for study of placental pathologies, Int. J. Mol. Sci. 21 (2020) 1–12, doi:10.3390/ijms21228755.
[28] C. Blundell, Y.S. Yi, L. Ma, E.R. Tess, M.J. Farrell, A. Georgescu, L.M. Aleksunes, D. Huh, Placental drug transport-on-a-chip: a microengineered in vitro model of transporter-mediated drug efflux in the human placental barrier, Adv. Healthc. Mater. 7 (2018) 1–9, doi:10.1002/adhm.201700786.
[29] R.L. Pemathilaka, J.D. Caplin, S.S. Aykar, R. Montazami, N.N. Hashemi, Placenta-on-a-chip: in vitro study of caffeine transport across placental barrier using liquid chromatography mass spectrometry, Glob. Challenges 3 (2019) 1800112, doi:10.1002/gch2.201800112.
[30] F. Yin, Y. Zhu, M. Zhang, H. Yu, W. Chen, J. Qin, A 3D human placenta-on-a-chip model to probe nanoparticle exposure at the placental barrier, Toxicol. Vitr. 54 (2019) 105–113, doi:10.1016/j.tiv.2018.08.014.
[31] P. Schuller, M. Rothbauer, S.R.A. Kratz, G. Höll, P. Taus, M. Schinnerl, J. Genser, N. Bastus, O.H. Moriones, V. Puntes, B. Huppertz, M. Siwetz, H. Wanzenböck, P. Ertl, A lab-on-a-chip system with an embedded porous membrane-based impedance biosensor array for nanoparticle risk assessment on placental Bewo trophoblast cells, Sens. Actuators B 312 (2020) 127946, doi:10.1016/j.snb.2020.127946.
[32] Y. Zhu, F. Yin, H. Wang, L. Wang, J. Yuan, J. Qin, Placental barrier-on-a-chip: modeling placental inflammatory responses to bacterial infection, ACS Biomater. Sci. Eng. 4 (2018) 3356–3363, doi:10.1021/acsbiomaterials.8b00653.
[33] D. Mandt, P. Gruber, M. Markovic, M. Tromayer, M. Rothbauer, S.R. Adam Kratz, S.F. Ali, J. Van Hoorick, W. Holnthoner, S. Mühleder, P. Dubruel, S. Van Vlierberghe, P. Ertl, R. Liska, A. Ovsianikov, Fabrication of biomimetic placental barrier structures within a microfluidic device utilizing two-photon polymerization, Int. J. Bioprint. 4 (2018) 1–12, doi:10.18063/IJB.v4i2.144.
[34] S. Miura, K. Sato, M. Kato-Negishi, T. Teshima, S. Takeuchi, Fluid shear triggers microvilli formation via mechanosensitive activation of TRPV6, Nat. Commun. 6 (2015) 1–11, doi:10.1038/ncomms9871.
[35] M.W. Toepke, D.J. Beebe, PDMS absorption of small molecules and consequences in microfluidic applications, Lab Chip 6 (2006) 1484–1486, doi:10.1039/b612140c.
[36] C.S. Roland, J. Hu, C.E. Ren, H. Chen, J. Li, M.S. Varvoutis, L.W. Leaphart, D.B. Byck, X. Zhu, S.W. Jiang, Morphological changes of placental syncytium and their implications for the pathogenesis of preeclampsia, Cell. Mol. Life Sci. 73 (2016) 365–376, doi:10.1007/s00018-015-2069-x.
[37] B.P. Lüscher, C. Marini, M.S. Joerger-Messerli, X. Huang, M.A. Hediger, C. Albrecht, M.U. Baumann, D.V. Surbek, Placental glucose transporter (GLUT)-1 is down-regulated in preeclampsia, Placenta 55 (2017) 94–99, doi:10.1016/j.placenta.2017.04.023.
[38] P. Vulto, S. Podszun, P. Meyer, C. Hermann, A. Manz, G.A. Urban, Phaseguides: a paradigm shift in microfluidic priming and emptying, Lab Chip 11 (2011) 1596–1602, doi:10.1039/c0lc00643b.
[39] C.M. Oefner, A. Sharkey, L. Gardner, H. Critchley, M. Oyen, A. Moffett, Collagen type IV at the fetal-maternal interface, Placenta 36 (2015) 59–68, doi:10.1016/j.placenta.2014.10.012.
[40] V.van Duinen Zonneveld, W. Stam, V. Borgdorff, A. Reijerkerk, V. Orlova, P. Vulto, T. Hankemeier, Standardized and scalable assay to study perfused 3d angiogenic sprouting of IPSC-derived endothelial cells *in vitro*, J. Vis. Exp. 2019 (2019) 1–11, doi:10.3791/59678.
[41] S.K. Gupta, S.S. Malhotra, A. Malik, S. Verma, P. Chaudhary, Cell signaling pathways involved during invasion and syncytialization of trophoblast cells, Am. J. Reprod. Immunol. 75 (2016) 361–371, doi:10.1111/aji.12436.
[42] W. Omata, W.E. Ackerman IV, D.D. Vandre, J.M. Robinson, Trophoblast cell fusion and differentiation are mediated by both the protein kinase C and A pathways, PLoS One 8 (2013) 1–12, doi:10.1371/journal.pone.0081003.
[43] A. Schröpfer, U. Kammerer, M. Kapp, J. Dietl, S. Feix, J. Anacker, Expression pattern of matrix metalloproteinases in human gynecological cancer cell lines, BMC Cancer 10 (2010) 553, doi:10.1186/1471-2407-10-553.
[44] M. Raeeszadeh-Sarmazdeh, L.D. Do, B.G. Hritz, Metalloproteinases and their inhibitors: potential for the development of new therapeutics, cells 9 (2020) 1–34, doi:10.3390/cells9051313.
[45] S. Ricard-Blum, The collagen family, Cold Spring Harb. Perspect. Biol. 3 (2011) 1–19, doi:10.1101/cshperspect.a004978.
[46] C.M. Luchian I, A. Goriuc, D. Sandu, The role of matrix metalloproteinases (MMP-8, MMP-9, MMP-13) in periodontal and peri-implant pathological processes, Int. J. Mol. Sci. 23 (2022) 1806, doi:10.3390/ijms23031806.
[47] S.J. Trietsch, E. Naumovska, D. Kurek, M.C. Setyawati, M.K. Vormann, K.J. Wilschut, H.L. Lanz, A. Nicolas, C.P. Ng, J. Joore, S. Kustermann, A. Roth, T. Hankemeier, A. Moisan, P. Vulto, Membrane-free culture and real-time barrier integrity assessment of perfused intestinal epithelium tubes, Nat. Commun. 8 (2017) 1–7, doi:10.1038/s41467-017-00259-3.
[48] J. Schindelin, I. Arganda-Carreras, E. Frise, V. Kaynig, M. Longair, T. Pietzsch, S. Preibisch, C. Rueden, S. Saalfeld, B. Schmid, J.Y. Tinevez, D.J. White, V. Hartenstein, K. Eliceiri, P. Tomancak, A. Cardona, Fiji: an open-source platform for biological-image analysis, Nat. Methods. 9 (2012) 676–682, doi:10.1038/nmeth.2019.
[49] A. Nicolas, F. Schavemaker, K. Kosim, D. Kurek, M. Haarmans, M. Bulst, K. Lee, S. Wegner, T. Hankemeier, J. Joore, K. Domansky, H.L. Lanz, P. Vulto, S.J. Trietsch, High throughput transepithelial electrical resistance (TEER) measurements on perfused membrane-free epithelia, Lab Chip 21 (2021) 1676–1685, doi:10.1039/d0lc00770f.
[50] S.M. Pizer, E.P. Amburn, J.D. Austin, R. Cromartie, A. Geselowitz, T. Greer, B. ter Haar Romeny, J.B. Zimmerman, K. Zuiderveld, Adaptive histogram equalization and its variations, Comput. Vis. Graph. Image Process 39 (1987) 355–368, doi:10.1016/S0734-189X(87)80186-X.
[51] H. Nazeran, F. Rice, W. Moran, J. Skinner, Biomedical image processing in pathology: a review, Australas. Phys. Eng. Sci. Med. 18 (1995) 26–38.
[52] E.S. Gedraite, M. Hadad, Investigation on the effect of a Gaussian Blur in image filtering and segmentation, Proc. Elmar - Int. Symp. Electron. Mar (2011) 393–396.
[53] T.W. Ridler, S. Calvard, Picture thresholding using an iterative selection method, IEEE Trans. Syst. Man Cybern. smc-8 (1978) 630–632, doi:10.1109/TSMC.1978.4310039.
[54] J. Vriend, T.T.G. Nieskens, M.K. Vormann, B.T. van den Berge, A. van den Heuvel, F.G.M. Russel, L. Suter-Dick, H.L. Lanz, P. Vulto, R. Masereeuw, M.J. Wilmer, Screening of drug-transporter interactions in a 3D microfluidic renal proximal tubule on a chip, AAPS J. 20 (2018) 87, doi:10.1208/s12248-018-0247-0.
[55] E.M. Leslie, Q. Mao, C.J. Oleschuk, R.G. Deeley, S.P.C. Cole, Modulation of multidrug resistance protein 1 (MRP1/ABCC1) transport and ATpase activities by interaction with dietary flavonoids, Mol. Pharmacol. 59 (2001) 1171–1180, doi:10.1124/mol.59.5.1171.
[56] J.J. Van Zanden, H.M. Wortelboer, S. Bijlsma, A. Punt, M. Usta, P.J.V. Bladeren, I.M.C.M. Rietjens, N.H.P. Cnubben, Quantitative structure activity relationship studies on the flavonoid mediated inhibition of multidrug resistance proteins 1 and 2, Biochem. Pharmacol. 69 (2005) 699–708, doi:10.1016/j.bcp.2004.11.002.
[57] M.L. Amin, P-glycoprotein inhibition for optimal drug delivery, Drug Target Insights 2013 (2013) 27–34, doi:10.4137/DTI.S12519.
[58] K.M. Bircsak, C.J. Gibson, R.W. Robey, L.M. Aleksunes, Assessment of drug transporter function using fluorescent cell imaging, Curr. Protoc. Toxicol. 1 (2013) 1–22, doi:10.1002/0471140856.tx2306s57.
[59] M.R. Syme, J.W. Paxton, J.A. Keelan, Drug transfer and metabolism by the human placenta, Clin. Pharmacokinet. 43 (2004) 487–514, doi:10.2165/00003088-200443080-00001.
[60] K.M. Włoch S, A. Pałasz, Active and passive transport of drugs in the human placenta, Ginekol. Pol. 80 (2009) 772–777.
[61] M. Yang, Z.M. Lei, C.V. Rao, The central role of human chorionic gonadotropin in the formation of human placental syncytium, Endocrinology 144 (2003) 1108–1120, doi:10.1210/en.2002-220922.
[62] C. Esnault, S. Priet, D. Ribet, C. Vernochet, T. Bruls, C. Lavialle, J. Weissenbach, T. Heidmann, A placenta-specific receptor for the fusogenic, endogenous retrovirus-derived, human syncytin-2, Proc. Natl. Acad. Sci. U. S. A. 105 (2008) 17532–17537, doi:10.1073/pnas.0807413105.
[63] G.M. Pacifici, R. Nottoli, Placental transfer of drugs administered to the mother, Clin. Pharmacokinet. 28 (1995) 235–269, doi:10.2165/00003088-199528030-00005.
[64] P.W. Lebedeva IV, P. Pande, Sensitive and specific fluorescent probes for functional analysis of the three major types of Mammalian ABC transporters, PLoS One 6 (2011) e22429, doi:10.1371/journal.pone.0022429.
[65] J.P.G. Eric M George, Recent insights into the pathophysiology of preeclampsia, Expert Rev. Obstet. Gynecol. 5 (2010) 557–556, doi:10.1586/eog.10.45.
[66] K. Chau, A. Hennessy, A. Makris, Placental growth factor and pre-eclampsia, J. Hum. Hypertens. 31 (2017) 782–786, doi:10.1038/jhh.2017.61.
[67] R. Soundararajan, A.J. Rao, Trophoblast 'pseudo-tumorigenesis': significance and contributory factors, Reprod. Biol. Endocrinol. 12 (2004) 1–12, doi:10.1186/1477-7827-2-15.
[68] J.-Y. Zhu, Z.-J. Pang, Y.-H. Yu, Regulation of trophoblast invasion: the role of matrix metalloproteinases, Rev. Obstet. Gynecol. 5 (2012) e137–e143, doi:10.3909/riog0196.
[69] R.E. Al-Enazy S, S. Ali, N. Albekairi, M. El-Tawil, Placental control of drug delivery, Adv. Drug. Deliv. Rev. (2017) 63–72, doi:10.1016/j.addr.2016.08.002.
[70] V. Costanzo, A. Bardelli, S. Siena, S. Abrignani, Exploring the links between cancer and placenta development, Open Biol 8 (2018), doi:10.1098/rsob.180081.
[71] B.A. Pelaseyed T, Regulation of actin-based apical structures on epithelial cells, J. Cell Sci. (2018), doi:10.1242/jcs.221853.
[72] I. Zwaenepoela, A. Nabaa, M.M. Lyra Da Cunhab, L. Del Maestroa, E. Formstecherc, D. Louvarda, M. Arpina, Ezrin regulates microvillus morphogenesis by promoting distinct activities of Eps8 proteins, Mol. Biol. Cell. 23 (2012) 1080–1094, doi:10.1091/mbc.E11-07-0588.
[73] M.R. Khushali Patel, Jasmine Nguyen, Sumaiyah Shaha, Amy Brightwell, Wendy Duan, Ashley Zubkowski, Loss of polarity regulators initiates gasdermin E mediated pyroptosis in human maternal fetal interface trophoblasts, Biorxiv (2023), doi:10.1101/2022.06.30.498172.
[74] C.W. Smarason, A.K. Sargent, I.L. Starkey, P. Redman, The effect of placental syncytiotrophoblast microvillous membranes from normal and pre-eclamptic women on the growth of endothelial cells *in vitro*, BJOG 101 (1994) 559–559, doi:10.1111/j.1471-0528.1994.tb13171.x.
[75] J.D. Boyd, W.J. Hamiltont, C.A.R. Boydi, The surface of the syncytium of the human chorionic villus, J. Anat. 102 (1968) 553–563.
[76] C.A.R. Boyd, Review: epithelial aspects of human placental trophoblast, Placenta 34 (2013) 11–13, doi:10.1016/j.placenta.2012.11.013.
[77] G. Pidoux, Spatiotemporal regulation of cAMP signaling controls the human trophoblast fusion, 6 (2015) 1–14. 10.3389/fphar.2015.00202.
[78] M. Rothbauer, N. Patel, H. Gondola, M. Siwetz, A comparative study of five

physiological key parameters between four different human trophoblast-derived cell lines, Sci. Rep. (2017) 1–11, doi:10.1038/s41598-017-06364-z.
[79] E. Lecarpentier, A. Atallah, J. Guibourdenche, M. Hebert-Schuster, S. Vieille-fosse, A. Chissey, B. Haddad, G. Pidoux, D. Evain-Brion, A. Barakat, T. Fournier, V. Tsatsaris, Fluid shear stress promotes placental growth factor upregulation in human syncytiotrophoblast through the cAMP-PKA signaling pathway, Hypertension 68 (2016) 1438–1446, doi:10.1161/HYPERTENSIONAHA.116.07890.
[80] M. Castellucci, I. Classen-Linke, J. Mühlhauser, P. Kaufmann, L. Zardi, R. Chiquet-Ehrismann, The human placenta: a model for tenascin expression, Histochemistry 95 (1991) 449–458, doi:10.1007/BF00315740.
[81] M.H. Hans-Peter Hohn, Larry R. Boots, Hans-Werner Denker, Differentiation of human trophoblast cells *in vitro* stimulated by extracellular matrix, Placenta 14 (1993) 181–200, doi:10.1016/S0143-4004(05)80293-0.
[82] K.P. Demir R, G. Kosanke, G. Kohnen, S. Kertschanska, Classification of human placental stem villi: review of structural and functional aspects, Microsc. Res. Tech. 38 (1997) 29–41, doi:10.1002/(SICI)1097-0029(19970701/15)38:1/2<29::AID-JEMT5>3.0.CO;2-P.
[83] F. Liu, M.J. Soares, K.L. Audus, Permeability properties of monolayers of the human trophoblast cell line BeWo, Am. J. Physiol. 273 (1997) 1596–1604, doi:10.1152/ajpcell.1997.273.5.c1596.
[84] M.V. St.-Pierre, M.A. Serrano, R.I.R. Macias, U. Dubs, M. Hoechli, U. Lauper, P.J. Meier, J.J.G. Marin, Expression of members of the multidrug resistance protein family in human term placenta, Am. J. Physiol. 279 (2000) 1495–1503, doi:10.1152/ajpregu.2000.279.4.r1495.
[85] C. Biondi, M.E. Ferretti, L. Lunghi, S. Medici, F. Cervellati, B. Pavan, F. Vesce, D. Morano, E. Adinolfi, F. Bertoni, L. Abelli, cAMP efflux from human trophoblast cell lines: a role for multidrug resistance protein (MRP)1 transporter, Mol. Hum. Reprod. 16 (2010) 481–491, doi:10.1093/molehr/gaq023.
[86] J.S. Gilbert, M.J. Ryan, B.B. Lamarca, M. Sedeek, S.R. Murphy, J.P. Granger, Pathophysiology of hypertension during preeclampsia: linking placental ischemia with endothelial dysfunction, Am. J. Physiol. 294 (2008) 718–722, doi:10.1152/ajpheart.01113.2007.
[87] Y. Zhang, H. jun Zhao, X. ru Xia, F. yang Diao, X. Ma, J. Wang, L. Gao, J. Liu, C. Gao, Y. gui Cui, J. yin Liu, Hypoxia-induced and HIF1α-VEGF-mediated tight junction dysfunction in choriocarcinoma cells: implications for preeclampsia, Clin. Chim. Acta 489 (2019) 203–211, doi:10.1016/j.cca.2017.12.010.
[88] C.J. Jones, An ultrastructural and ultrahistochemical study of the human placenta in maternal essential hypertension, Placenta 1 (1981) 61–76, doi:10.1016/s0143-4004(80)80016-6.
[89] A.N. Sharp, A.E.P. Heazell, D. Baczyk, C.E. Dunk, H.A. Lacey, C.J.P. Jones, J.E. Perkins, J.C.P. Kingdom, P.N. Baker, I.P. Crocker, Preeclampsia is associated with alterations in the p53-pathway in villous trophoblast, PLoS One 9 (2014) 1–14, doi:10.1371/journal.pone.0087621.
[90] H. Arnholdt, F. Meisel, K. Fandrey, U. Löhrs, Proliferation of villous trophoblast of the human placenta in normal and abnormal pregnancies, Virchows Arch. B Cell Pathol. Incl. Mol. Pathol. 60 (1991) 365–372, doi:10.1007/BF02899568.
[91] R.W. Redline, P. Patterson, Pre-eclampsia is associated with an excess of proliferative immature intermediate trophoblast, Hum. Pathol. 26 (1995) 594–600, doi:10.1016/0046-8177(95)90162-0.
[92] L.J. Bailey, S. Alahari, A. Tagliaferro, M. Post, I. Caniggia, Augmented trophoblast cell death in preeclampsia can proceed via ceramide-mediated necroptosis, Cell Death. Dis. 8 (2017) 1–14, doi:10.1038/cddis.2016.483.
[93] Y. Kudo, C.A.R. Boyd, I.L. Sargent, C.W.G. Redman, Hypoxia alters expression and function of syncytin and its receptor during trophoblast cell fusion of human placental BeWo cells: implications for impaired trophoblast syncytialisation in pre-eclampsia, Biochim. Biophys. Acta 1638 (2003) 63–71, doi:10.1016/S0925-4439(03)00043-7.
[94] C. Wich, S. Kausler, J. Dotsch, W. Rascher, I. Knerr, Syncytin-1 and glial cells missing a: hypoxia-induced deregulated gene expression along with disordered cell fusion in primary term human trophoblasts, Gynecol. Obstet. Invest. 68 (2009) 9–18, doi:10.1159/000209396.
[95] S.R. Langbein M, R. Strick, P.L. Strissel, N. Vogt, H. Parsch, M.W. Beckmann, Impaired cytotrophoblast cell–cell fusion is associated with reduced syncytin and increased apoptosis in patients with placental dysfunction, Mol. Reprod. Dev. 75 (2008) 175–183.
[96] F. Lyall, S.C. Robson, J.N. Bulmer, Spiral artery remodeling and trophoblast invasion in preeclampsia and fetal growth restriction relationship to clinical outcome, Hypertension 62 (2013) 1046–1054, doi:10.1161/HYPERTENSIONAHA.113.01892.
[97] B.O. Asvold, L.J. Vatten, T.G. Tanbo, A. Eskild, Concentrations of human chorionic gonadotrophin in very early pregnancy and subsequent pre-eclampsia: a cohort study, Hum. Reprod. 29 (2014) 1153–1160, doi:10.1093/humrep/deu068.
[98] M. Liu, Y. Yin, H. Yu, R. Zhou, Laminins regulate placentation and pre-eclampsia: focus on trophoblasts and endothelial cells, Front. Cell Dev. Biol. 8 (2020) 1–8, doi:10.3389/fcell.2020.00754.
[99] F.E.I. Liu, M.J. Soares, K.L. Audus, M.J. Soares, K.L. Audus, Permeability properties of monolayers of the human trophoblast cell line BeWo, (2022) 1596–1604.
[100] K. Orendi, M. Gauster, G. Moser, H. Meiri, B. Huppertz, The choriocarcinoma cell line BeWo: syncytial fusion and expression of syncytium-specific proteins, Reproduction 140 (2010) 759–766, doi:10.1530/REP-10-0221.
[101] B. Novakovic, L. Gordon, N.C. Wong, A. Moffett, U. Manuelpillai, J.M. Craig, A. Sharkey, R. Saffery, Wide-ranging DNA methylation differences of primary trophoblast cell populations and derived cell lines: implications and opportunities for understanding trophoblast function, Mol. Hum. Reprod. 17 (2011) 344–353, doi:10.1093/molehr/gar005.
[102] D.A. Evseenko, J.W. Paxton, J.A. Keelan, ABC drug transporter expression and functional activity in trophoblast-like cell lines and differentiating primary trophoblast, Am. J. Physiol. 290 (2006) R1357–R1365, doi:10.1152/ajpregu.00630.2005.
[103] Y. Hagiwara, H. Kumagai, N. Ouwerkerk, L. Gijzen, R. Annida, M. Bokkers, R. van Vught, K. Yoshinari, Y. Katakawa, K. Motonaga, T. Tajiri, A novel in vitro membrane permeability methodology using three-dimensional Caco-2 tubules in a microphysiological system which better mimics in vivo physiological conditions, J. Pharm. Sci. 111 (2022) 214–224, doi:10.1016/j.xphs.2021.11.016.
[104] M. Horii, Y. Li, A.K. Wakeland, D.P. Pizzo, K.K. Nelson, K. Sabatini, L.C. Laurent, Y. Liu, M.M. Parast, Human pluripotent stem cells as a model of trophoblast differentiation in both normal development and disease, Proc. Natl. Acad. Sci. U. S. A. 113 (2016) E3882–E3891, doi:10.1073/pnas.1604747113.
[105] Z. Li, O. Kurosawa, H. Iwata, Establishment of human trophoblast stem cells from human induced pluripotent stem cell-derived cystic cells under micromesh culture, Stem Cell Res. Ther. 10 (2019) 1–14, doi:10.1186/s13287-019-1339-1.
[106] M.A. Sheridan, R.C. Fernando, L. Gardner, M.S. Hollinshead, G.J. Burton, A. Moffett, M.Y. Turco, Establishment and differentiation of long-term trophoblast organoid cultures from the human placenta, Nat. Protoc. 15 (2020) 3441–3463, doi:10.1038/s41596-020-0381-x.
[107] R. Aouache, L. Biquard, D. Vaiman, F. Miralles, Oxidative stress in preeclampsia and placental diseases, Int. J. Mol. Sci. 19 (2018), doi:10.3390/ijms19051496.